AFRL-AFOSR-JP-TR-2024-0037

Investigating instability mechanisms and their impacts on the coupled solar wind-magnetosphere-ionosphere (SW-M-I) system

ILDIKO HORVATH
THE UNIVERSITY OF QUEENSLAND
THE UNIVERSITY OF QUEENSLAND
ST LUCIA, , 4072
AUS

01/03/2024
Final Technical Report

Air Force Research Laboratory
Air Force Office of Scientific Research
Asian Office of Aerospace Research and Development
Unit 45002, APO AP 96338-5002

REPORT DOCUMENTATION PAGE

PLEASE DO NOT RETURN YOUR FORM TO THE ABOVE ORGANIZATION.

1. REPORT DATE	2. REPORT TYPE	3. DATES COVERED	
20240103	Final	START DATE 20210929	END DATE 20230928

4. TITLE AND SUBTITLE
Investigating instability mechanisms and their impacts on the coupled solar wind-magnetosphere-ionosphere (SW-M-I) system

5a. CONTRACT NUMBER	5b. GRANT NUMBER	5c. PROGRAM ELEMENT NUMBER
	FA2386-21-1-4103	61102F
5d. PROJECT NUMBER	**5e. TASK NUMBER**	**5f. WORK UNIT NUMBER**

6. AUTHOR(S)
Ildiko Horvath

7. PERFORMING ORGANIZATION NAME(S) AND ADDRESS(ES)
THE UNIVERSITY OF QUEENSLAND
THE UNIVERSITY OF QUEENSLAND
ST LUCIA 4072
AUS

8. PERFORMING ORGANIZATION REPORT NUMBER

9. SPONSORING/MONITORING AGENCY NAME(S) AND ADDRESS(ES)	10. SPONSOR/MONITOR'S ACRONYM(S)	11. SPONSOR/MONITOR'S REPORT NUMBER(S)
AOARD UNIT 45002 APO AP 96338-5002	AFRL/AFOSR IOA	AFRL-AFOSR-JP-TR-2024-0037

12. DISTRIBUTION/AVAILABILITY STATEMENT
A Distribution Unlimited: PB Public Release

13. SUPPLEMENTARY NOTES

14. ABSTRACT
The various instability mechanisms [such as Kelvin-Helmholtz (K-H), Rayleigh-Taylor (R-T), interchange] are closely related and significantly impact the coupled solar wind-magnetosphere-ionosphere (SW-M-I) system. Important members of this coupled system include the hot zone along with the various subauroral flows known as Sub-Auroral Ion Drifts (SAID), Sub-Auroral Polarization Streams (SAPS), SAPS wave structures (SAPSWS), Abnormal SAID (ASAID), and Double-peak SAID (DSAID). During this project, we conducted a series of detailed studies documented in journal articles. Based on M-I conjugate observations, we analyzed (i) the fast-time development of the various newly-formed subauroral flows observed during the various magnetic local time (MLT) hours of interest by invoking the novel short-circuiting theory, (ii) the hot zone and its structuring by the reflected K-H waves generated by the SW-driven K-H vortices rolling along the magnetopause or by the plasma density dropouts caused by the ongoing magnetic field line stretching occurring during the underlying magnetotail reconnection events, (iii) the various inner-magnetosphere configurations associated with the fast-time development of ASAID, often accompanied by SAID during multiple flow channel development, and (iv) the various polar convection patterns underlying the various subauroral flow channels in the various MLT sectors of interest. Our respective new findings include (i) the dawnside development of SAPS flow channel, (ii) the Near-Earth Plasma Sheet (NEPS) acting as a resonator after activation by the K-H vortices on the magnetopause and generating reflected (from the plasmapause) K-H waves structuring the hot zone, (iii) the single intrusion and repeated intrusions of hot ring current ions into the cold plasmasheet plasma leading to the respective development of single ASAID flow channel and multiple ASAID flow channels, and (iv) the antisunward streaming SAID flows in the postmidnight MLT sector along with the dawnward intruded dusk cell related antisunward convection flows, the antisunward streaming ASAID flows in the postmidnight sector against the dawn cell related sunward convection flows, and the development of enhanced SAPS flows in the midnight sector amplified by the dusk cell related convection flows. The new results obtained contribute to the better understanding of (a) some basic geophysical processes by explaining some fundamental multiple inter-relationships and configurations leading to the structuring of the hot zone by K-H waves or by plasma density dropouts due to magnetic field line stretching and (b) the subauroral flows forming complex patterns on the duskside or appearing on the dawnside as sunward or antisunward flows. To demonstrate the significance of the new results obtained, one of the journal articles published was featured as an Editor's Highlight in the recently published Eos Science News: ttps://eos.org/research-spotlights/probing-rare-hot-plasma-flows-in-the-upper-atmosphere.

15. SUBJECT TERMS

16. SECURITY CLASSIFICATION OF:			17. LIMITATION OF ABSTRACT	18. NUMBER OF PAGES
a. REPORT	b. ABSTRACT	c. THIS PAGE		
U	U	U	SAR	27

19a. NAME OF RESPONSIBLE PERSON	19b. PHONE NUMBER *(Include area code)*
GEOFFREY ANDERSEN	703-588-8442

Section 1: Structured Survey Questions

Award Information:

Award Number: FA2386-21-1-4103
Report Type: Final Performance
Principal Investigator: HORVATH, ILDIKO
Principal Investigator Email: ihorvath@eecs.uq.edu.au
Principal Investigator Phone: +61 7 336 51643
Project Title: Investigating instability mechanisms and their impacts on the coupled solar wind-magnetosphere-ionosphere (SW-M-I) system
Recipient Organization: THE UNIVERSITY OF QUEENSLAND
Business Office Email: geoffrey.andersen.4@us.af.mil
Report Due Date: 12/27/2023
Report Period Start Date: 09/29/2012
Report Period End Date: 09/28/2023
Current Program Officer: ANDERSEN, GEOFFREY
Please list any other Co-Program Officers (if applicable): N/A

Publications:

1) Horvath, I., & Lovell, B. C. (2022). Newly formed dawnside, duskside, and nightside subauroral flows developed during magnetically active times. *Journal of Geophysical Research: Space Physics*, 127(10), e2021JA030215. https://doi.org/10.1029/2021JA030215
2) Horvath, I., & Lovell, B. C. (2023). Abnormal Sub-Auroral Ion Drifts (ASAID) developed in various inner-magnetosphere configurations at geomagnetically quiet times. *Journal of Geophysical Research: Space Physics*, 128(1), e2022JA031004. https://doi.org/10.1029/2022JA031004
3) Horvath, I., & Lovell, B. C. (2023). Sub-auroral flows and associated magnetospheric and ionospheric phenomena developed during 7–8 September 2017. *Journal of Geophysical Research: Space Physics, 128(3)*, e2022JA030966. https://doi.org/10.1029/2022JA030966
4) Horvath, I., & Lovell, B. C. (2023). Sub-Auroral Ion Drifts (SAID) developed over the northern winter hemisphere at dawn during 2016-2017. *Journal of Geophysical Research: Space Physics, 128(4)*, e2022JA031228. https://doi.org/10.1029/2022JA031228
5) Horvath, I., & Lovell, B. C. (2023). Antisunward streaming westward sub-auroral ion drifts (SAID) developed in the postmidnight (1-4) magnetic local time sector during 2013. *Journal of Geophysical Research: Space Physics, 128(9)*, e2023JA031677. https://doi.org/10.1029/2023JA031677 (JGR Space Physics Editor's highlight)
6) Horvath, I., & Lovell, B. C. (2023). Abnormal Sub-Auroral Ion Drifts (ASAID) developed in the postmidnight (1–4) magnetic local time sector in 2013. *Journal of Geophysical Research: Space Physics, 128(9)*, e2023JA031808. https://doi.org/10.1029/2023JA031808
7) Horvath, I., & Lovell, B. C. (2023). Intense westward Sub-Auroral Polarization Streams (SAPS) developed in the premidnight-postmidnight (23-2) magnetic local time sector during 2015 and 2016. *Journal of Geophysical Research: Space Physics* (under review)

Participants: N/A
Other Partners or Collaborators: N/A
Inventions, patent applications, licenses, and technologies/techniques: Nothing to report

Section 2: Technical Report

2 Accomplishments

2.1 Research Objectives of this project

The hot zone is regarded as the most important region of interest for understanding the development and maintenance of various subauroral flows. These flows include the Sub-Auroral Ion Drifts (SAID Spiro et al., 1979; Anderson et al., 1991), Sub-Auroral Polarization Streams (SAPS Foster & Burke, 2002), SAPS wave structures (SAPSWS; Mishin et al., 2003), Abnormal SAID (ASAID; Voiculescu & Roth, 2008), and Double-peak SAID (DSAID; He et al., 2016). In order to contribute to the better understanding of these subauroral flows, this project focused on the various geophysical mechanisms (including instability mechanisms) impacting the hot zone and leading to subauroral flow channel (FC) formation.

The main objective of this project was to investigate in detail how the various geophysical and instability mechanisms impact the hot zone and the subauroral, auroral, and polar regions. Our major goal was to investigate the coupled solar wind-magnetosphere-ionosphere (SW-M-I) system for driver-response mechanisms in order to understand (1) how the hot zone becomes structured or impacted by the various geophysical and instability mechanisms under magnetically quiet and active conditions, (2) what sort of subauroral flows, auroral forms, and polar features develop due to these impacts, and (3) what are the underlying driver mechanisms.

We obtained new results by employing and correlating multi-satellite and multi-instrument data and by constructing and analyzing correlated observations of (i) the hot zone in the inner magnetosphere and (ii) the various subauroral flows, auroral forms and polar features in the topside ionosphere By integrating the new results and findings into the existing and evolving theories, this project provided new insights and an improved understanding of the physical mechanisms underlying the coupled SW-M-I system. Understanding M-I coupled plasma jets and their plasma environment is significant because of the severe impacts on propagating radio waves -causing satellite/radar signal scintillations and dropouts- adversely affecting the auroral-middle latitude range (Mishin & Blaunstein, 2008; Nishimura et al., 2021). Such importance is exemplified by the recent advancements made in observations (Sinevich et al., 2023; Nishimura et al., 2023) and in modeling (Mishin & Streltsov, 2023) reproducing fine-scale structures caused by ionospheric feedback instability (IFI; Mishin & Streltsov, 2019) mechanisms. Thus, project outcomes benefit current studies and research efforts at the AFRL and NRL, and add to the MURI (Multidisciplinary University Research Initiative) project. To exemplify the significance of some of the new findings obtained, one of the published articles became highlighted by the Editor of Journal of Geophysical Research Space Physics.

2..2 Details of accomplishments during this project

2.2.1 Introduction

The hot zone (Gingauze & Bezrukikh, 1976) is the plasmasphere's outer region ($L>3\ R_E$) where (i) the plasmasheet's earthward inner edge and the ring current's outer edge overlap (Frank, 1971), (ii) the ion temperature (Gingauze & Bezrukikh, 1976) is high compared with the plasmasphere's inner region ($L<3\ R_E$), (iii) the electron temperature (Décréau et al., 1982) becomes also elevated, and (iv) the temperature (ion and electron) rapidly changes with increasing L values. According to recent studies (Mishin & Streltsov, 2021 and references therein), the hot zone is regarded as the most important region of interest for understanding the development and maintenance of duskside and nightside subauroral flows such as SAPS and SAID.

According to the fast-time generation theory put forward by recent studies based on observational evidence (Mishin, 2013, Mishin et al., 2017, Mishin & Streltsov, 2020, 2021), SAID and SAPS develop on a short time scale and the newly-formed M-I conjugate SAID and SAPS FCs collocate with ring current injections, since the subauroral ionosphere maps to the overlapping ring current/plasmasheet region in the inner magnetosphere (Phul-Quinn et al., 2007). Thus, SAID and SAPS development starts in the magnetosphere and is related to the propagation of mesoscale plasma flows (MPFs) into the plasmasphere (Mishin & Puhl-Quinn, 2003, Mishin et al., 2010; Mishin, 2013; Mishin et al., 2017). MPFs (i.e. plasma injections related to bursty bulk flows

(BBFs) originating from the magnetotail reconnection site) propagate into the inner magnetosphere and form the properties of plasmasheet (Sergeev et al., 1999). As the earthward propagating MPFs-related hot electrons become stopped at the plasmapause (when the electron density reaches ~10 cm^{-3}), the MPFs-related hot ions move further inward until they become stopped by the developing outward polarization E field near the plasmapause (Mishin & Sotnikov, 2017). In the nightside equatorial magnetosphere, this outward polarization E field maps down to the subauroral ionosphere as a poleward polarization E field and drives the sunward (westward) SAID and SAPS flows. The newly-formed SAPS/SAID FC is located (i) on the plasma density trough's poleward boundary and shows no clear relation to the underlying plasma density and conductivity, (ii) at the electron aurora's equatorward edge forming a dispersionless cutoff, and (iii) within the substorm-injected auroral ion precipitation regime appearing with an equatorward drop-off that marks the SAPS/SAID FC's equatorward edge.

2.2.2 Methodology

In this project, we conducted a series of detailed studies investigating the various subauroral FCs' and associated ionospheric features' development unfolding in various magnetic local time (MLT) sectors and under various geomagnetic conditions. We focused on the FCs' newly-formed state and on those MLT sectors that are less investigated and therefore less understood. These include the dawn sector and the near midnight sector.

Since the subauroral FCs' development starts in the inner magnetosphere, we utilized M-I conjugate observations provided by the magnetosphere Time History of Events and Macroscale Interactions during Substorms (THEMIS) and Van Allen Probes (VAP) satellites observing the plasmapause and its environment and by the topside-ionosphere Defense Meteorological Satellite Program (DMSP) spacecraft.

For specifying the events of interest, we surveyed many years of DMSP zonal drift velocity plots. We surveyed the DMSP F15 plots for the calendar year of 2015 and specified 21 postmidnight (1-4 MLT) ASAID events and 13 postmidnight (1-4 MLT) SAID events, and also for the calendar years of 2015-2016 and specified 24 near-midnight (23-2 MLT) SAPS events. We also surveyed the DMSP F16 plots for the calendar year of 2015 and specified 6 dawnside (~6 MLT) SAID events and for the calendar years of 2016-2017 and specified 15 dawnside (3-6 MLT) SAID events observed over the northern winter hemisphere. Finally, we also investigated the various inner-magnetosphere configurations underlying the development of ASAID during geomagnetically quiet times and the 7-8 September 2017 intense (SYM-Hmin=-146 nT) geomagnetic storm for the various inner magnetosphere and topside ionosphere features.

2.2.3 Results and Discussion

2.2.3.1 Newly-formed dawnside, duskside, and nightside subauroral flows developed during magnetically active times

In this study, we investigated a series of newly-formed (with an upper limit of ~101 min) subauroral flows, as evidenced by their associated ring current (RC) injections and proton precipitations (Mishin & Phul-Quinn; 2003). These flows include a newly-formed dawnside broad subauroral FC and, for the first time, the newly-formed dawnside (~5-6 MLT) rapid narrow subauroral flows. We also investigated the newly-formed duskside broad SAPS flows at ~15 MLT and the newly-formed nightside narrow SAID flows at ~19-20 MLT. With the observations presented, we demonstrated the basic characteristics of the newly-formed dusk/nightside and dawnside subauroral flows. Based on the observational evidence presented, we specified the dawnside rapid narrow subauroral flows as the sunward (westward) SAID developed in the dawn sector (as shown in Figure 1) and the dawnside broad subauroral FC as the dawnside sunward (eastward) SAPS (as shown in Figure 2): the dawnside equivalent of the duskside sunward (westward) SAPS associated with downward region 2 (R2) field-aligned currents (FACs). Further evidence includes the inner-magnetosphere observations of the hot zone both on the dusk/nightside and on the dawnside (as shown in Figure 3).

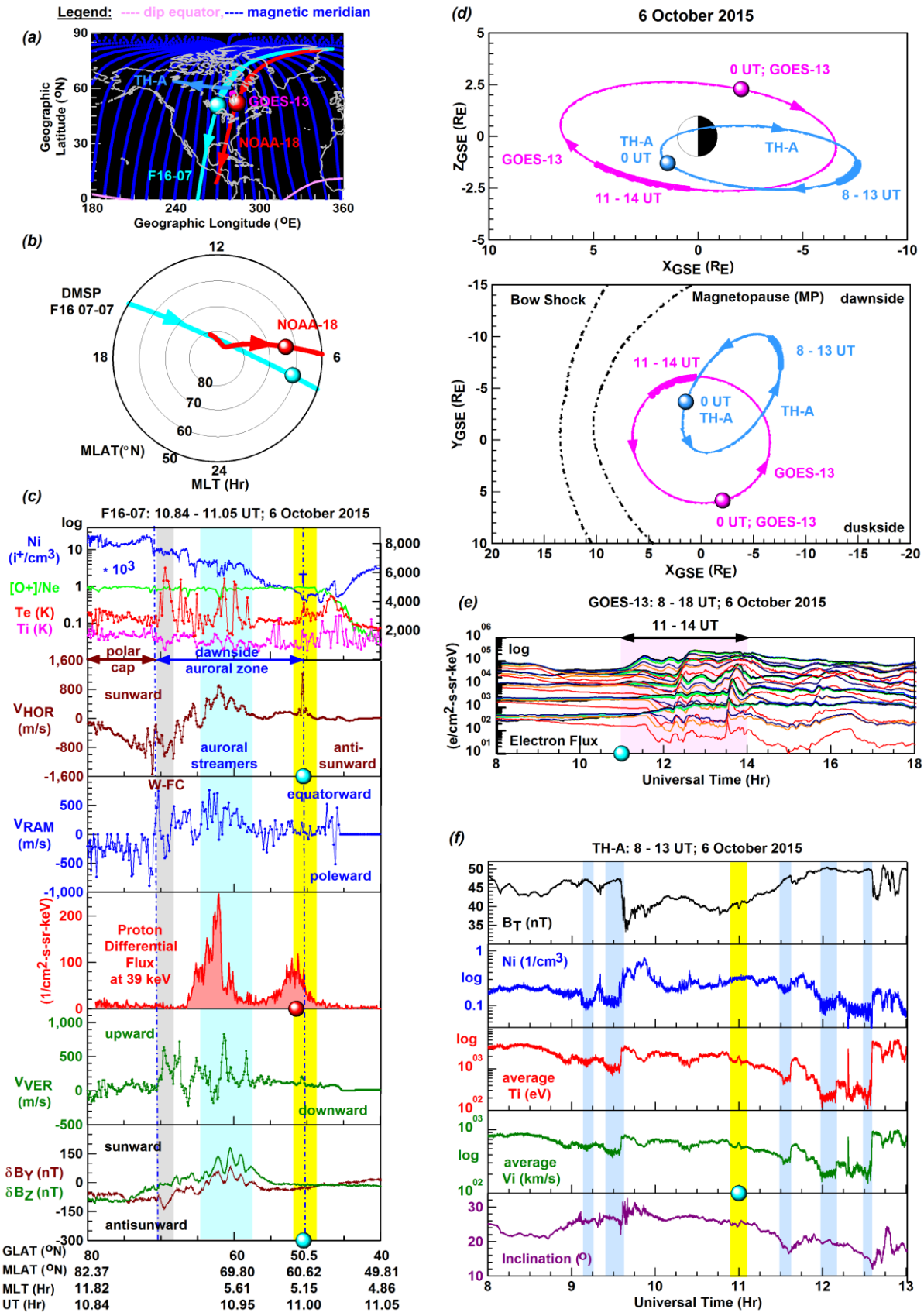

Figure 1 shows on the dawnside the newly-formed sunward streaming westward SAID flow (driven by the poleward SAID E field) in the dawn sector on 6 October 2015 and its plasma environment.

Figure 1 illustrates the newly-formed sunward (westward) SAID developed on the dawnside on the magnetically moderate (Kp<4) day of 6 October 2016. In panel (a), the northern-hemisphere

map illustrates the correlated ground-tracks of the dawnside descending passes of DMSP F16 (in cyan) and NOAA-18 (in red) and the footprints of the THEMIS-A (TH-A; in light blue) and GOES-13 (in magenta) satellites. In panel (b), the MLT versus MLAT polar map depicts the locations of these satellite passes along with the sunward (westward) SAID FC (dot in cyan) and localized subauroral proton peak (dot in red) appearing at similar magnetic latitudes on the dawnside. In panel (c), the DMSP F16 and NOAA-18 line-plot sets illustrate (i) the sunward (westward) SAID flow (shaded interval in yellow; V_{HOR}≈1,400 m/s) developed on the dawnside (at ~5-6 MLT) and appeared in the regime of substorm-injected RC ions evidencing its newly-formed state and (ii) the equatorward propagating auroral streamers (shaded interval in cyan) in the dawnside auroral zone. These auroral streamers, the ionospheric signatures (i.e. auroral footprints) of the BBFs released from the magnetotail reconnection site (Lyons et al., 1999; Fairfield et al., 1999), occurred during this dawnside SAID event implying the diversion of BBFs to the dawnside. The diversions of BBFs imply also the formation of both the substorm current wedge (SCW) and the R1-R2 FACs (Birn et al., 2004; Keiling et al. 2009). Thus, the RC protons had been carried and injected earthward by the MPFs (Fok et al., 1996), originating from the BBFs, and the earthward injected MPFs became short-circuited across the dawnside plasmapause just like on the duskside across the duskside plasmapause (Mishin & Puhl-Quinn, 2007). In panel (d), the orbit plots depict the orbit sections of interest (highlighted sections; GOES-13 in magenta; TH-A in light blue) located below the magnetic equatorial plane and on the dawnside, and away from the magnetopause. In panel (e), the line plots of GOES-measured electron flux illustrate a series of particle injections (shaded interval in light magenta) during the time period of interest. In the dawn sector, the newly-formed sunward (westward) SAID FC (marked as dot in cyan) was detected during these particle injections. In panel (f), the TH-A line plots, covering the time period of interest, show a series of plasma density dropouts (indicated by the decreased ion density (Ni) and ion temperature (Ti) and ion velocity (Vi) and low inclination ($I<30^o$; shaded intervals in light blue). As marked (dot in cyan; shaded interval in yellow), the newly-formed dawnside sunward (westward) SAID FC was observed between two sets (an earlier set and a latter set) of flux dropout events.

Figure 2 is constructed the same way as Figure 1 and illustrates a newly-formed dawnside broad SAPS FC detected under storm conditions (Kp=8-) on 17 March 2015 by the DMSP F16 satellite just before 5 MLT. Panels (a-b) show the correlated descending F16 and NOAA-15 passes near Alaska tracking the dawnside broad SAPS flows (marked as dot in cyan) and associated dawnside localized proton flux increase (marked as dot in red) at ~50 magnetic latitude (MLAT) evidencing the dawnside SAPS flows' newly-formed state. In panel (c), the DMSP F16 line plot sets illustrate the dawnside SAPS flows (shaded interval in yellow; V_{HOR}≈1,500 m/s) appearing within the mid-latitude trough's poleward half and in the regime of dawnside upward R2 FACs that connected with the dawnside dawnward R1 FACs at the equatorward edge of the dawnside auroral zone via the dawnside equatorward directed ionospheric Pedersen currents. In the dawnside auroral zone, a dawnside auroral arc (shaded interval in cyan) appeared wherein the dawnside downward R1 and upward R2 FACs connected with equatorward Pedersen currents and drove strong eastward drifts streaming sunward and reaching V_{HOR}≈4,000 m/s. Meanwhile, the upward drift varied in a similar fashion. Within the dawnside auroral arc, the equatorward drift maximized at V_{RAM}≈2,000 m/s. As the correlated NOAA-15 proton differential flux line plot shows (in panel (c)), substantial localized increases occurred on the dawnside: at subauroral [1.8×10^5 (1/cm^2-s-str-keV)] and auroral [6.2×10^6 (1/cm^2-s-str-keV)] latitudes under storm conditions. These demonstrate that both the dawnside broad SAPS flows and the dawnside auroral arc were associated with trapped RC protons. Shown in panels (d-e), GOES-13 observed on the duskside a series of particle injections during the time interval of interest (shaded interval in light magenta) when the newly-formed dawnside broad SAPS FC (dot in cyan) was tracked. As shown in panel (f) with the VAP-A line plot sets, the newly-formed dawnside broad sunward (eastward) SAPS FC was associated with stretched magnetic field lines ($I<10^o$) as evidenced by the Ne dropouts detected by VAP-A, but on the duskside, as the orbit plots show in panel (d).

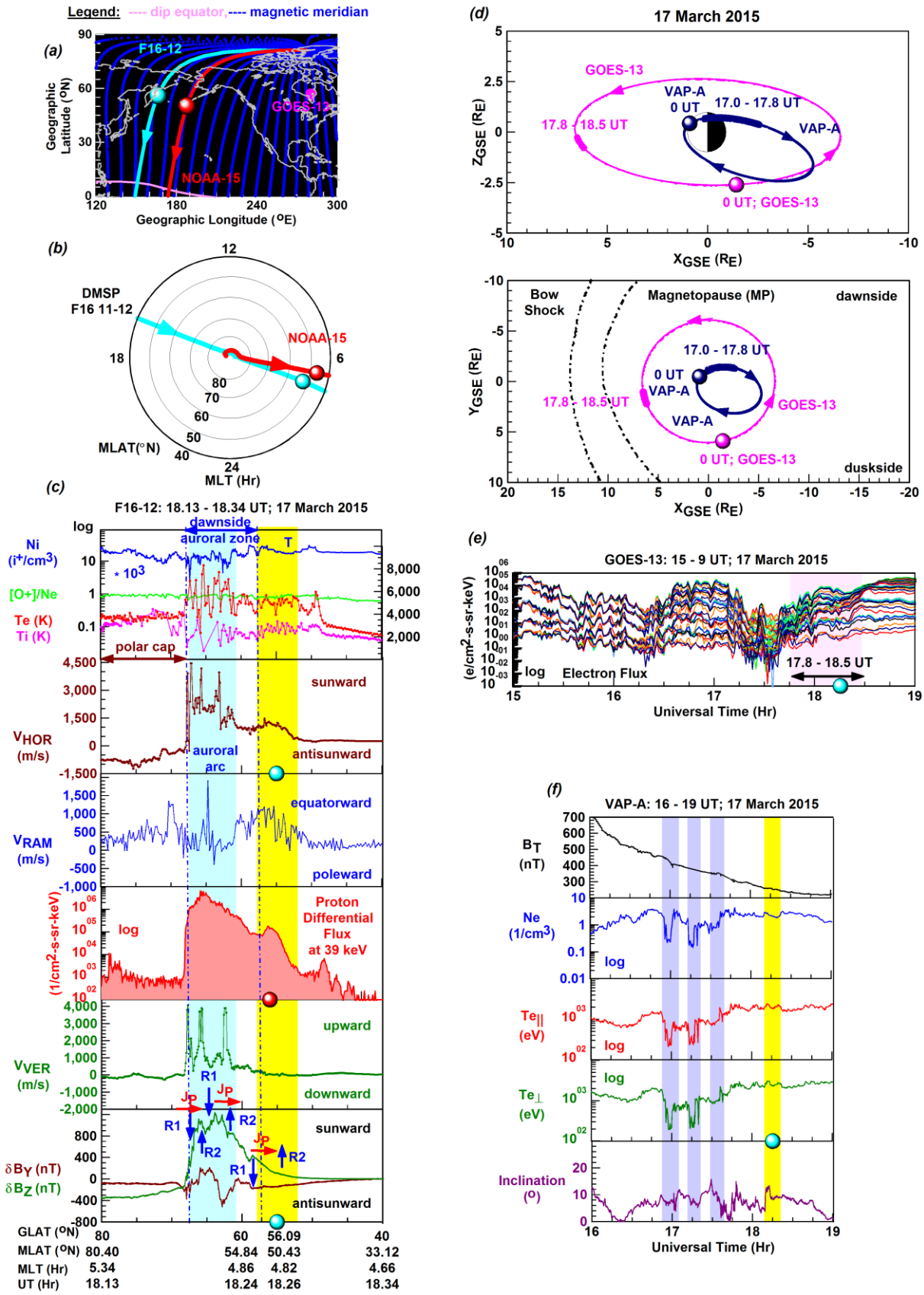

Figure 2 shows on the dawnside the newly-formed sunward streaming eastward SAPS flow (driven by the dawnside equatorward SAPS E field) in the dawn sector on 17 March 2015 and its plasma environment.

Figure 3 illustrates the hot zone developed on the duskside during the 17 March 2015 dropouts event observed by VAP-A (as shown in panel (a)) and on the dawnside during the 1 January 2016

dawnside SAID event observed by VAP-B (as shown in panel (d)). Panels (a-b) show the duskside hot zone (shaded interval in light green) depicted by the increased plasma density and temperature that became highly structured because of the electron dropouts occurring due to the magnetic field line stretching in the tail region. The hot zone extended from 3 to 6.5 R_E in the dusk-nighttime sector (18-22 MLT) revealing that the electron dropouts caused its structuring. Then, the duskside duskward and outward SAPS E field components (dot in green; shaded interval in yellow) were tracked at 55.26 MLAT and 18.27 MLT. Panels (c-d) illustrate the hot zone on the dawnside (shaded interval in light green) during the 1 January 2016 dawnside sunward (westward) SAID event. Then, the dawnside hot zone was situated outward of the dawnside plasmapause (between 7 and 11 R_E), appeared in the regime of elevated proton temperature and was highly structured (both in Ne and in Te). The dawnside duskward and outward SAID E field components (dot in dark orange; shaded interval in yellow) were observed at 6.81 MLT and 52.50 MLAT.

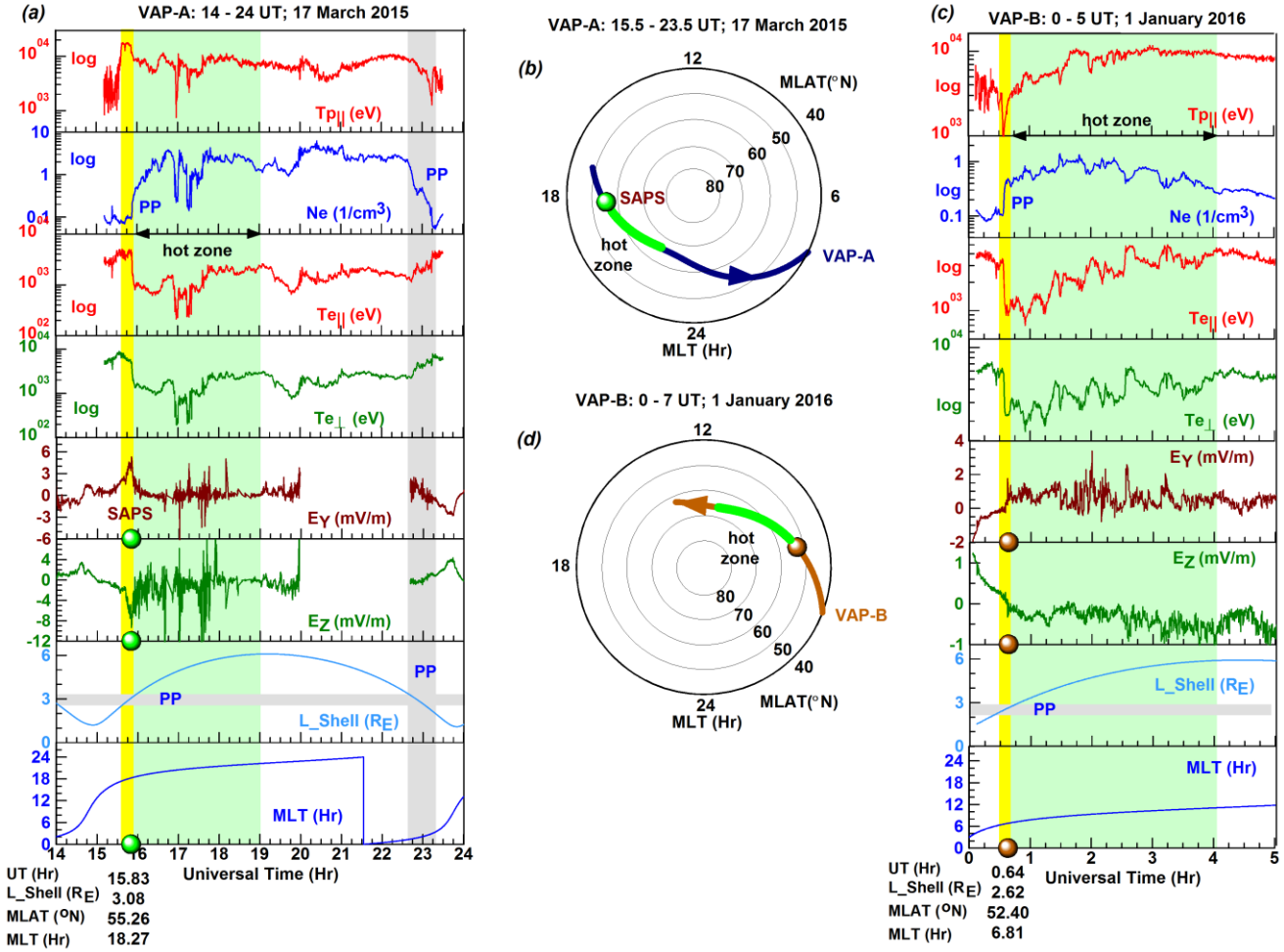

Figure 3: The VAP line plots depict the structured hot zone (shaded interval in light green) on the (a) duskside and (c) dawnside along with the (a) duskside SAPS E field components and (c) dawnside SAID E field components (duskward; $E_Y>0$ and outward; $E_Z<0$). Each polar plot shows the VAP satellite's ground track with the locations of E field (dot in color) and hot zone (highlighted section in light green) on the (b) dusk side and (d) dawn side.

For the time period investigated we concluded that the unfolding magnetic field line stretching (leading to plasma density dropouts) promoted the development of both: (1) the duskside and dawnside subauroral flows by creating favorable conditions for the MPFs' deeper earthward movement, which is crucial for short-circuiting, and (2) the structured hot zone both (i) on the dusk and nightside along with the duskward and outward SAPS E field components and (ii) on the dawnside along with the duskward and outward SAID E field components.

2.2.3.2 Sub-Auroral Ion Drifts (SAID) developed over the northern winter hemisphere at dawn during 2016-2017

In this study, we investigated the rare development of sunward streaming westward SAID FC in the topside ionosphere's dawn (3-6) MLT sector over the northern winter hemisphere. We surveyed the DMSP F16 data for the calendar years of 2016-2017 and found 7 SAID detections during 4.36-6.12 MLT in 2016 and 8 SAID detections during 3.79-5.60 MLT in 2017. But only a few matching inner-magnetosphere observations were found showing the duskward and outward SAID E field components. These provide observational evidence that the sunward (westward) SAID flows of the topside ionosphere in the dawn MLT sector were driven by the outward SAID E field, generated by short-circuiting (Mishin & Puhl-Quinn, 2007; Mishin, 2013), that mapped down to the topside ionosphere as a poleward SAID E field. New findings include the observations of localized heat source within the hot zone and near the newly-formed plasmapause, which develops in the 21-06 MLT sector (Heilig et al., 2022), and the dispersionless hot ion/proton injections across the localized heat source and in the hot zone. One example is shown in Figure 4.

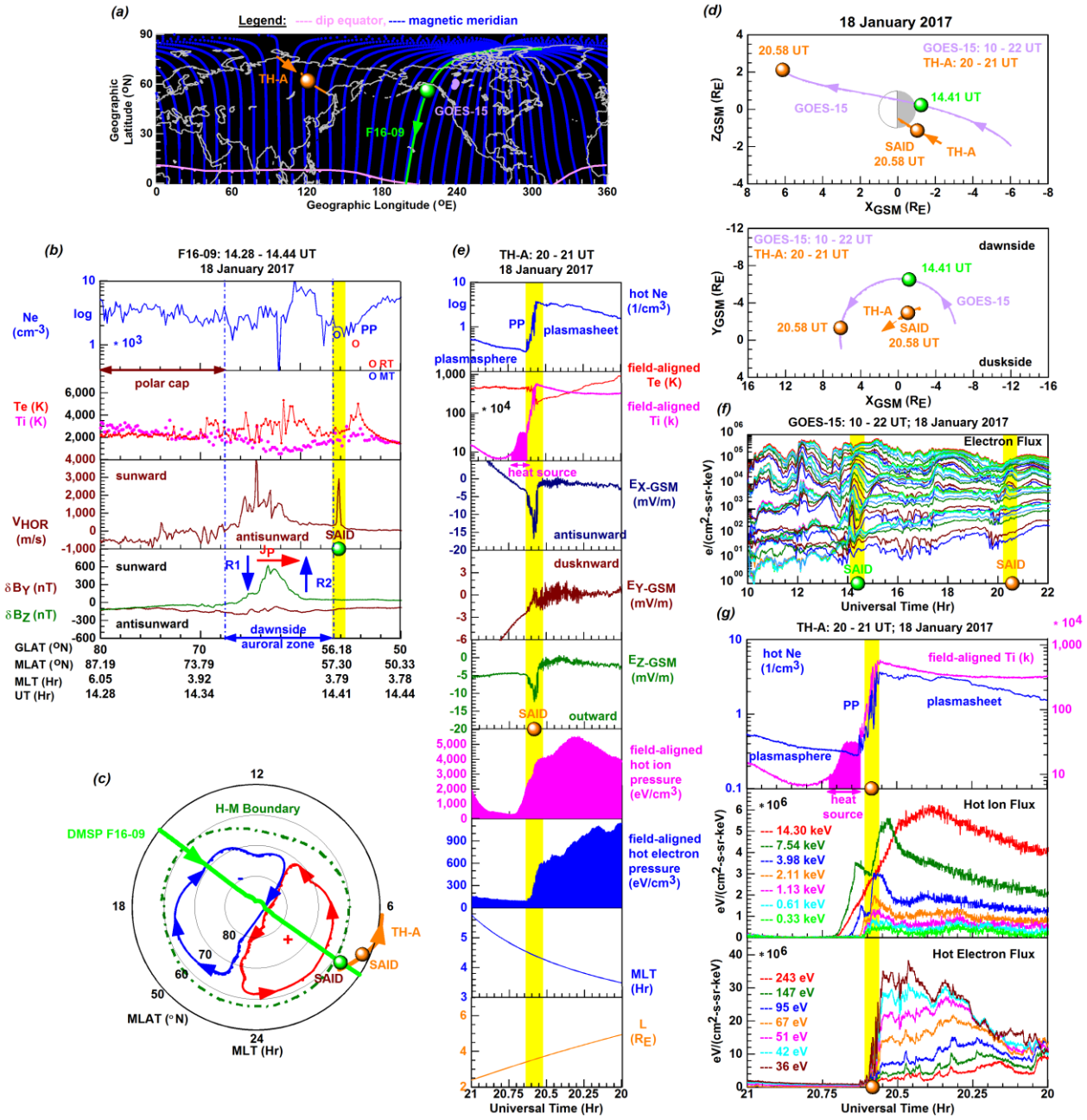

Figure 4 shows the 18 January 2017 sunward (westward) SAID event when the westward SAID flow (driven by the poleward SAID E field) was streaming sunward in concert with the dawn cell related sunward convection and when the hot zone developed on the earthward side.

Figure 4 shows the 18 January 2017 dawnside sunward (westward) SAID event. In panel (a), the northern-hemisphere map depicts the ground track of the DMSP F16 pass observing the SAID FC at dawn (marked as dot in green) and the footprints of the GOES-15 (in purple) and THEMIS-A (TH-A; in orange) orbit sections of interest. In panel (b), the DMSP F16 line plots show the sunward (westward) SAID flow (shaded interval in yellow) appearing equatorward of the dawnside auroral zone and the enhanced dawnside sunward auroral convection flow that was driven by the dawnside equatorward E field, as the associated equatorward Pedersen current (J_P; marked in red) connected the dawnside downward R1 and upward R2 FACs (marked in blue). But there were no dawnside upward R2 FACs flown at subauroral latitudes as the development of inner-magnetosphere outward SAID E field (mapped down to the ionosphere as a poleward SAID E field driving the westward SAID flows streaming sunward) was created by short-circuiting (Mishin & Phul-Quinn, 2007) and therefore independently of the large-scale R1-R2 FACs (Mishin, 2013). In panel (c), the MLT versus MLAT polar plot shows the prevailing two-cell polar convection operational, depicted by the dusk (in blue) and dawn (in red) cells and the tilted midday-midnight MLT axis (because of the IMF B_Y component) introducing a dawn-dusk asymmetry to the polar convection pattern (Ruohoniemi & Greenwald, 2005). Here, we plotted the SAID FC (dot in green) and SAID E field (dot in orange) locations appearing in the dawn sector and showing a close correlation in MLT and MLAT. In panel (d), the orbit plots show the orbit sections of interest and the SAID E field locations situated on the nightside below the magnetic equatorial plane and on the dawnside. In panel (e), the TH-A time series depict the outward SAID E field and the signatures of short circuiting. In panel (f) the GOES-13 line plots show a series of dispersionless particle injections at geostationary orbit (~6.6 R_E). As marked (shaded intervals in yellow), the injection events occurred during the SAID detections made by DMSP and TH-A. The injections' dispersionless nature provides observational evidence that GOES-15 was close to the injection region. Thus, the outward SAID E field on the dawnside developed during the ongoing injections of hot plasma (from the magnetotail reconnection site into the inner magnetosphere) creating favorable conditions to short-circuiting the hot MPFs across the cold plasmapause leading SAID development (Mishin & Puhl-Quinn, 2007; Mishin, 2013). Panel (g) shows a detailed illustration of the hot zone where the localized heat source developed earthward of the plasmapause that was newly-formed as implied by the dispersionless electron flux decreases (in the earthward direction) measured over a wide energy range (Su et al., 2018).

For the time period investigated we concluded that the dawnward extension of both (1) the reconnection-related RC injections and (2) the localized heat source across and near the newly-formed plasmapause resulted in the development of the (i) outward SAID E field by short-circuiting leading to the development of sunward (westward) SAID flows in the ionosphere's dawn (3-6 MLT) sector and (ii) downward heat flux in the inner magnetosphere leading to the development of the stable auroral red (SAR) arc (after Te was sufficiently high) in the ionosphere's dawn (3-6 MLT) sector.

2.2.3.3 Subauroral flows and associated magnetospheric and ionospheric phenomena developed during 7-8 September 2017

In this study, we investigated the 7-8 September 2017 geomagnetic storm (SYM-Hmin=-146 nT) during which a series of substorms occurred. For the specified five events (Events 1-5), we studied (i) the SAPS flows and (ii) the various magnetospheric E fields developed, and (iii) these E fields' plasma environment characterized by various geophysical phenomena. These included the particle dropouts in the magnetosphere near-Earth tail region, the Kelvin-Helmholtz (K-H) surface waves forming rolled-up vortices on the magnetopause, the Near-Earth Plasma Sheet (NEPS) acting as a resonator, and the hot zone near the plasmapause in the outer plasmasphere. Here, we highlight Event-5 demonstrating the simultaneous observations of (a) the K-H waves/vortices near the magnetopause, (b) the inner-magnetosphere hot zone that became structured by the reflected K-H waves near the plasmapause and (c) the various auroral forms observed in the topside ionosphere (as shown in Figures 5-6).

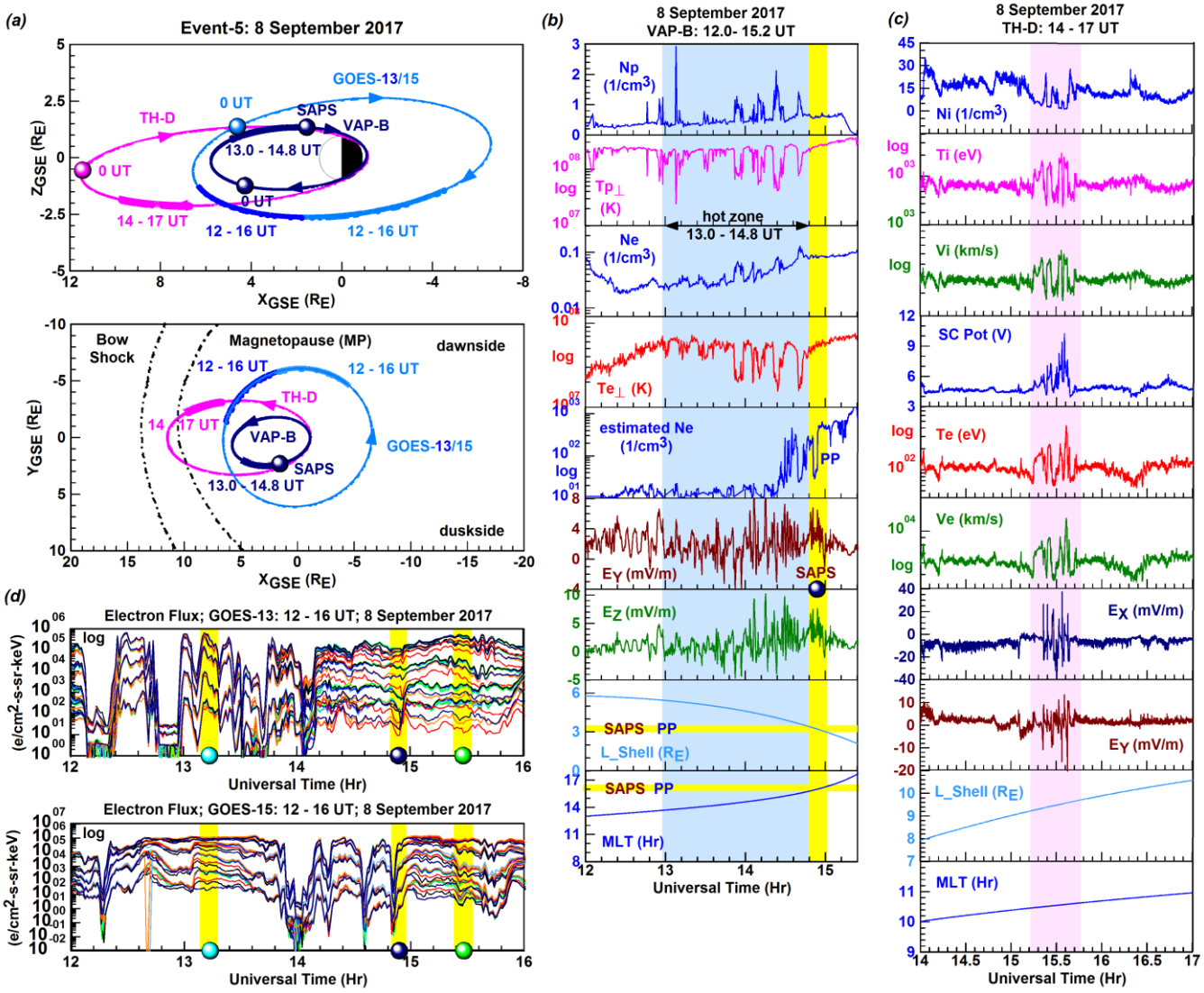

Figure 5 shows the various magnetosphere and inner-magnetosphere geophysical phenomena developed during Event-5.

Figure 5 is constructed for Event-5 and depicts the various geophysical phenomena observed in the inner magnetosphere (near the plasmapause) and in the magnetosphere (near the magnetopause). In panel (a), the orbit plots show the highlighted orbit sections of interest that had been completed during the recovery phase (under northward IMF and duskward IEF E_Y conditions) by GOES-13/15 (in blue), VAP-B (in dark blue) and TH-D (in magenta). As shown in panel (b), VAP-B crossed the plasmapause (PP; shaded interval in yellow) where the outward and duskward SAPS E field developed (dot in dark blue) and observed the hot zone (shaded interval in blue) that became structured by the reflected K-H surface waves in the NEPS resonator. The surface waves are depicted by the periodic variations of cold-dense and hot-tenuous plasma with T≈300s in the Pc5 (T=150-600s) range characteristic to K-H waves (Yumoto & Saito, 1980). Panel (c) shows that TH-D observed near the magnetopause the K-H vortices (shaded interval in light magenta) that activated the NEPS to act as a resonator. These K-H waves are depicted by the periodic (T≈180s) variations of the tenuous-hot-fast-moving magnetosphere plasma and dense-cold-slow-moving magnetosheath plasma in the Pc5 (T=150-600s) range. In panel (d), the two GOES satellites observed a series of dipolarization events with a series of sudden decreases followed by their respective sudden increases. These are the respective signatures of stretched magnetic field-line configurations (creating electron flux decreases) that became more dipole-like during the following magnetotail reconnection related particle injections (creating electron flux increases). As marked, the VAP-B-observed SAPS E field in the inner magnetosphere (dot in dark blue) and the

DMSP-observed SAPS flows in the topside ionosphere (dots in cyan and green) commonly appear in the regimes of high electron flux implying both dipole-like magnetic field line configurations and reconnection-related particle injections.

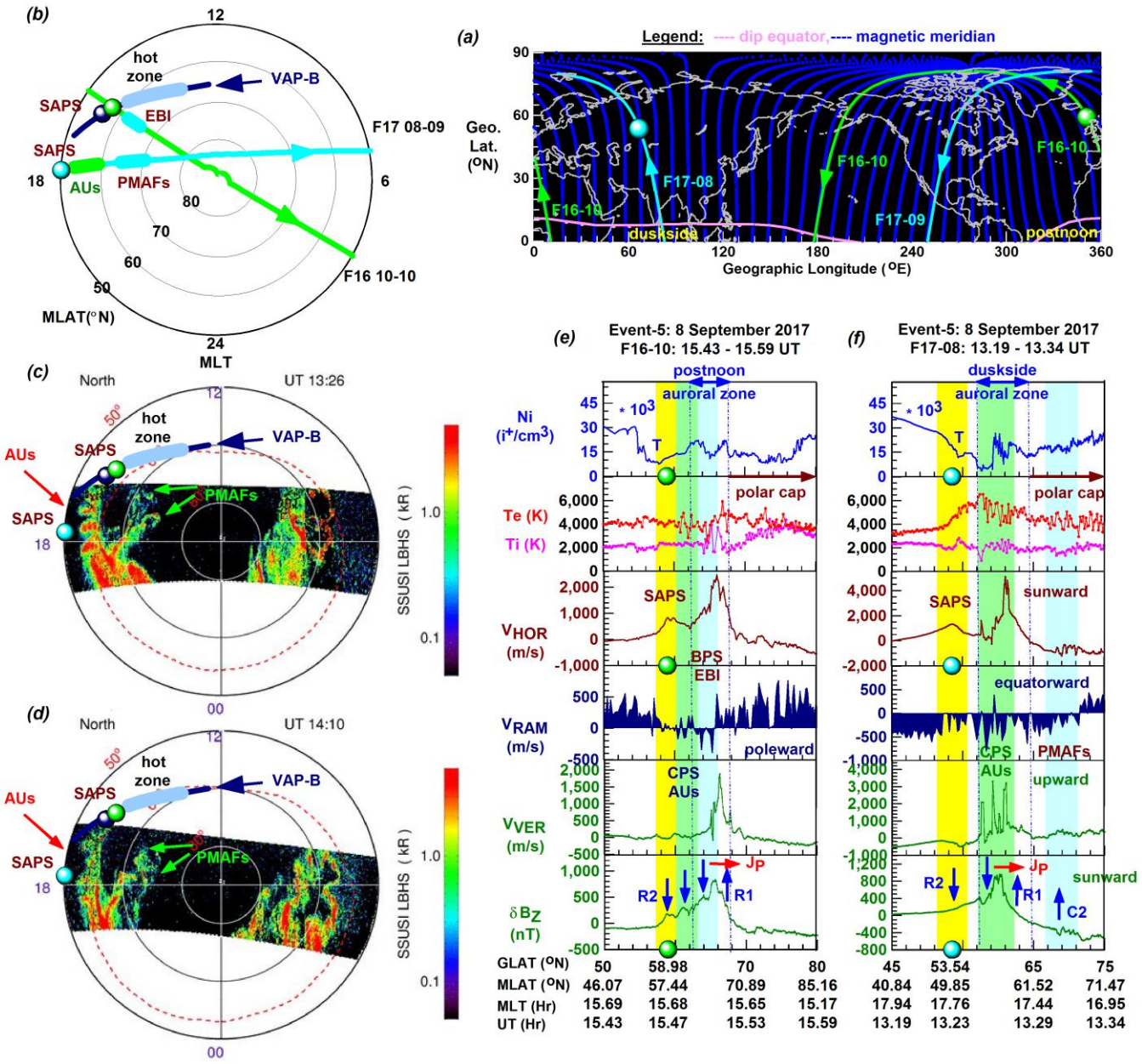

Figure 6 shows the various subauroral and auroral features observed in the topside ionosphere during Event-5.

Figure 6 is constructed for Event-5 and depicts the resultant ionospheric features observed in the topside ionosphere by DMSP F16 and 17. In panel (a), the northern-hemisphere map shows the F16 (in green) and F17 (in cyan) ground tracks and the locations of the sunward (westward) SAPS flows (dots in colors) observed. In panel (b), the MLT versus MLAT polar map shows that these SAPS flows developed in the dusk sector along with the various auroral features observed by DMSP (marked as highlighted sections in green and cyan). Here, we also mapped the locations of the hot zone (highlighted section in light blue) and outward SAPS E field (dot in dark blue) observed by VAP-B. In panels (c-d), the DMSP SUSSI images depict the various auroral features. These include (i) the auroral undulations (AUs) and (ii) the poleward moving auroral forms (PMAFs). As shown, the AUs and PMAFs were observed on the duskside (earlier at 13:26 UT and later on at 14:10 UT) and thus cover a larger time period of the hot zone observed by VAP-B

during 13.0-14.8 UT. In panels (e-f), the DMSP F16 and F17 line-plot sets depict the sunward (westward) SAPS flows (shaded interval in yellow) and the signatures of AUs (shaded interval in green) and PMAFs (shaded interval in cyan).

For the time period investigated, the new results include the demonstration of the simultaneous development of (i) the K-H waves/vortices near the magnetopause, (ii) the inner-magnetosphere hot zone that became structured by the reflected K-H waves near the plasmapause, and (iii) the various auroral forms such as AUs and PMAFs observed in the topside ionosphere. Findings (i)-(iii) provide further observations supporting the model of NEPS activation by K-H waves/vortices on the magnetopause (Leonovich & Mazure, 2005) and explanations of the concurrent events of hot zone structuring and auroral undulations. From these findings (i)-(iii) we concluded that the reflected K-H waves structured the hot zone and led auroral undulations.

2.2.3.4 Abnormal Sub-Auroral Ion Drifts (ASAID) developed in various inner-magnetosphere configurations at geomagnetically quiet times

In this study, we investigated a series of inner-magnetosphere configurations, some of them were suggested by Voiculescu & Roth (2008) and Voiculescu (2012), and one of them include the hot zone. We also analyzed ASAID development based on the recent fast-time short-circuiting theory put forward by Mishin & Puhl-Quinn (2007) for SAID development, and further studied the plasmasheet rippling scenario put forward by Horvath & Lovell (2019a, 2019b) based on the model of Maynard et al. (1996). Thus, we provided the required direct observational evidence with the observations of various inner-magnetosphere configurations and with the correlated ASAID observations obtained for the geomagnetically quiet (Kp≤ 3+) days of 30 November, and 7 and 9 December 2013. Here, we highlight the 9 December 2013 event (shown in Figure 7).

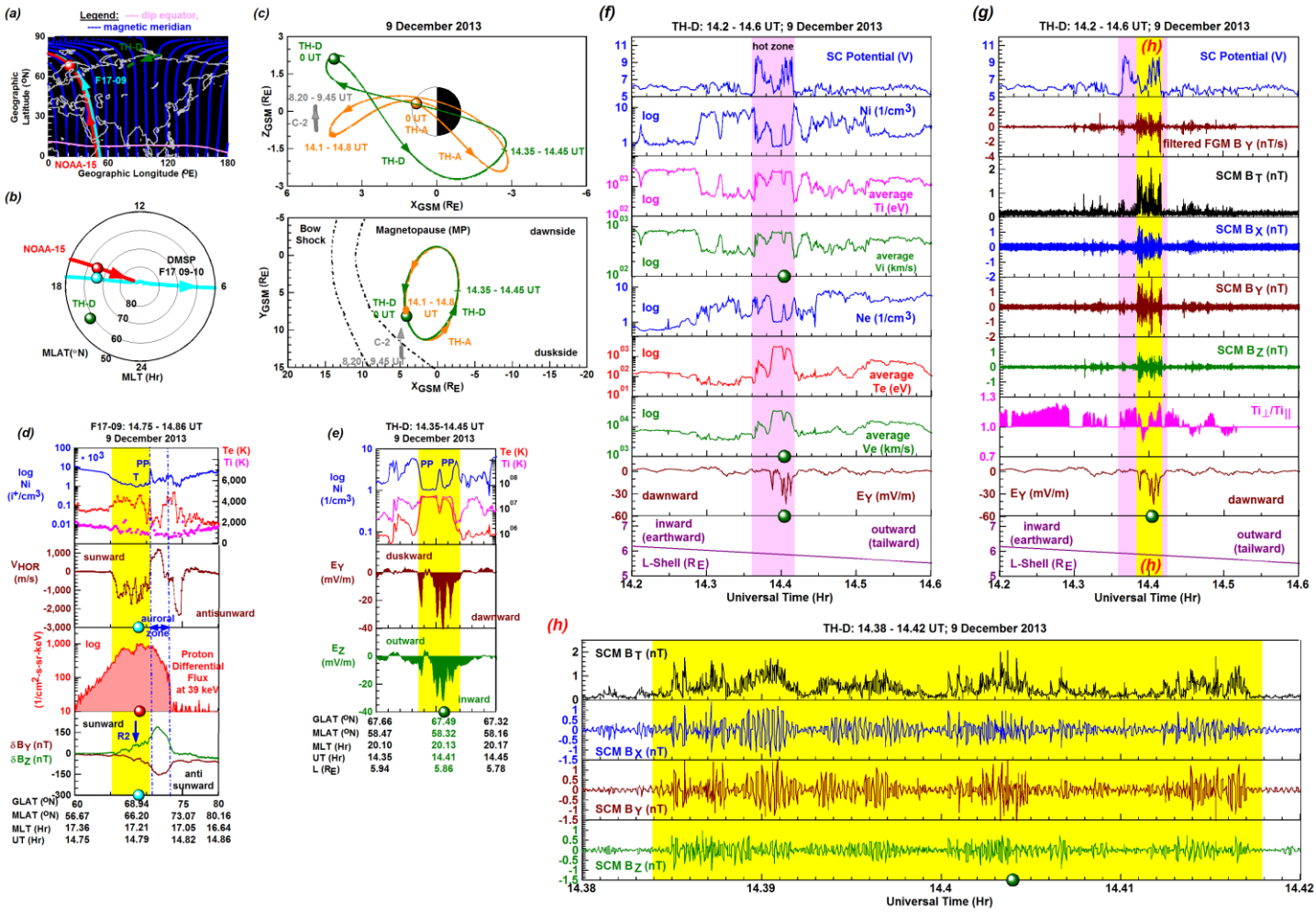

Figure 7 shows the more complex inner magnetosphere configuration observed by TH-D that led to the development of structured antisunward flows in the topside ionosphere detected by DMSP F17.

Figure 7 illustrates the configuration of hot-RC—cold-inner-edge-plasmasheet interface leading to the development of multiple ASAID channels observed by DMSP F17 in the topside ionosphere. In panel (a), northern-hemisphere map shows the close correlations of the DMSP F17 and NOAA-15 passes and the ASAID-related peaks (dots in colors) over Northern Europe and the TH-D footprints (in dark green) over Northern Asia. In panel (b), the MLT versus MLAT plot illustrates the ASAID flows observed by DMSP F17 and NOAA-15 in the dusk sector (~17 MLT) and by TH-D in the nighttime sector (~20 MLT). In panel (c), the TH-D orbit plots show that the multiple ASAID detections were made by TH-D over the southern hemisphere and close to the equatorial plane on the nightside and duskside. Thus, TH-D observed ASAID close the source region (i.e. close to the equatorial plane). In panel (d), the DMSP F17 and NOAA-15 line-plot sets depict the signature of multiple ASAID appearing in the topside ionosphere as a wide (~4^o) and structured antisunward FC (shaded interval in yellow) at 17.23 MLT where the antisunward (-) drifts reached ~-1,800 m/s. Within the structured antisunward FC, the NOAA-15 proton differential flux line plot depicts the locally enhanced precipitation of energetic protons (i.e. hot RC ions) appearing with undulations and thus implying RC injections and short-circuiting across the plasmapause in the inner magnetosphere. Panel (e) shows the TH-D-observed plasma environment of the ASAID E field and the inner-magnetosphere ASAID dawnward E_Y and inward E_Z components. Panel (f) illustrates a larger region of the inner magnetosphere where TH-D observed the hot zone (shaded interval in light magenta) and where the ASAID E field location situated within the hot zone is marked (dot in green). Within the hot zone, the plasma density (Ni and Ne) was structured showing multiple plasmapause signatures (Ne and Ni dropoffs) and depletions, while the average ion (Vi≈800 km/s) and electron (Ve≈3,300 km/s) drifts were highly elevated reaching supersonic values and thus implying that the hot zone was associated with the violation of diffusive equilibrium processes, as was concluded by the study of Vlasov & Tashkinova (1981). In panel (g), the TH-D line plot sets illustrate the signatures of intense waves, bounded by the steep SC potential gradients, that we specify as EMIC waves (Usanova et al., 2010). These time series illustrate the process of wave-particle interaction at work within the hot zone, where the hot RC ions with temperature anisotropy provided the energy for the generation of electromagnetic waves (i.e. EMIC waves) in the Pc1 range (T=0.2-5.0s; Jacobs & Watanabe, 1964). Panel (h) shows further details by depicting the quasi-periodic modulations of EMIC waves, as they became modulated by long-period ultralow frequency (ULF) waves on the same magnetic field lines and formed a series of Pc1 pearl structures (Troitskaya & Gul'Elmi, 1967).

For the various (simple and complex) inner-magnetosphere configurations investigated we concluded that ASAID developed due to short-circuiting and Larmor radius effects. While the simple inner-magnetosphere configuration led to the development of a single ASAID FC, the complex inner-magnetosphere configurations led to the development of complex subauroral channels or multiple ASAID FCs. During short-circuiting, the EMIC waves developed also promoted ASAID development since the interactions of hot energetic ions with the cold plasmasheet plasma are their common drivers. Such interactions commonly occur across the plasmapause during short-circuiting (Mishin & Puhl-Quinn, 2007), near the plasmapause during EMIC wave excitation on the duskside (Kozyra et al., 1997; Summers et al., 1998), and near/across the plasmapause in a certain inner magnetosphere configuration (Voiculescu & Roth, 2008; Voiculescu, 2012).

2.2.3.5 Antisunward streaming westward Sub-Auroral Ion Drifts (SAID) developed in the postmidnight (1-4) magnetic local time sector during 2013 (JGR Space Physics Editor's highlight)

In this study, we investigated the rare development of antisunward streaming westward SAID flows in the postmidnight (1-4 MLT) sector based on the 13 postmidnight SAID events occurred during the calendar year of 2013 and the underlying geomagnetic conditions. We studied the M-I conjugate SAID's (a) ionospheric environment based on DMSP F15 observations (see one example shown in Figure 8) and (b) inner-magnetosphere environment including the hot zone and underlying

heating mechanisms based on correlated SAID E field events observed by VAP-B in the inner magnetosphere (see examples shown in Figures 9 and 10).

Figure 8 shows the 10 July 2013 antisunward (westward) SAID event depicting the westward SAID flow streaming antisunward after magnetic midnight. The locations of DMSP F15 03-04 passes (in magenta) and antisunward (westward) SAID FC (dot in magenta) are shown by a series of maps. In panel (a), the southern-hemisphere map depicts the SAID FC over the South Atlantic. In panel (b), the MLT versus MLAT polar maps illustrate the polar two-cell convection pattern with the westward SAID FC streaming antisunward equatorward of the dawnward intruding dusk cell and therefore in concert with the dawnward intruding dusk cell related convection. In panel (c), the AMPERE generated polar map shows the large-scale upward (in red) and downward (in blue) FAC pattern with no downward R2 currents near the SAID FC as SAID development does not require large-scale FACs (Mishin, 2013). In panel (d) the DMSP SSUSI image shows the auroral precipitation in the dusk cell and the location of SAID FC situated equatorward of the auroral precipitation regime. In panel (e), the F15 time series depict the plasma environment of the SAID FC (shaded interval in yellow) and the signatures of antisunward (shaded interval in cyan) and sunward (shaded interval in light blue) dusk-cell-related convection flows in the postmidnight auroral zone.

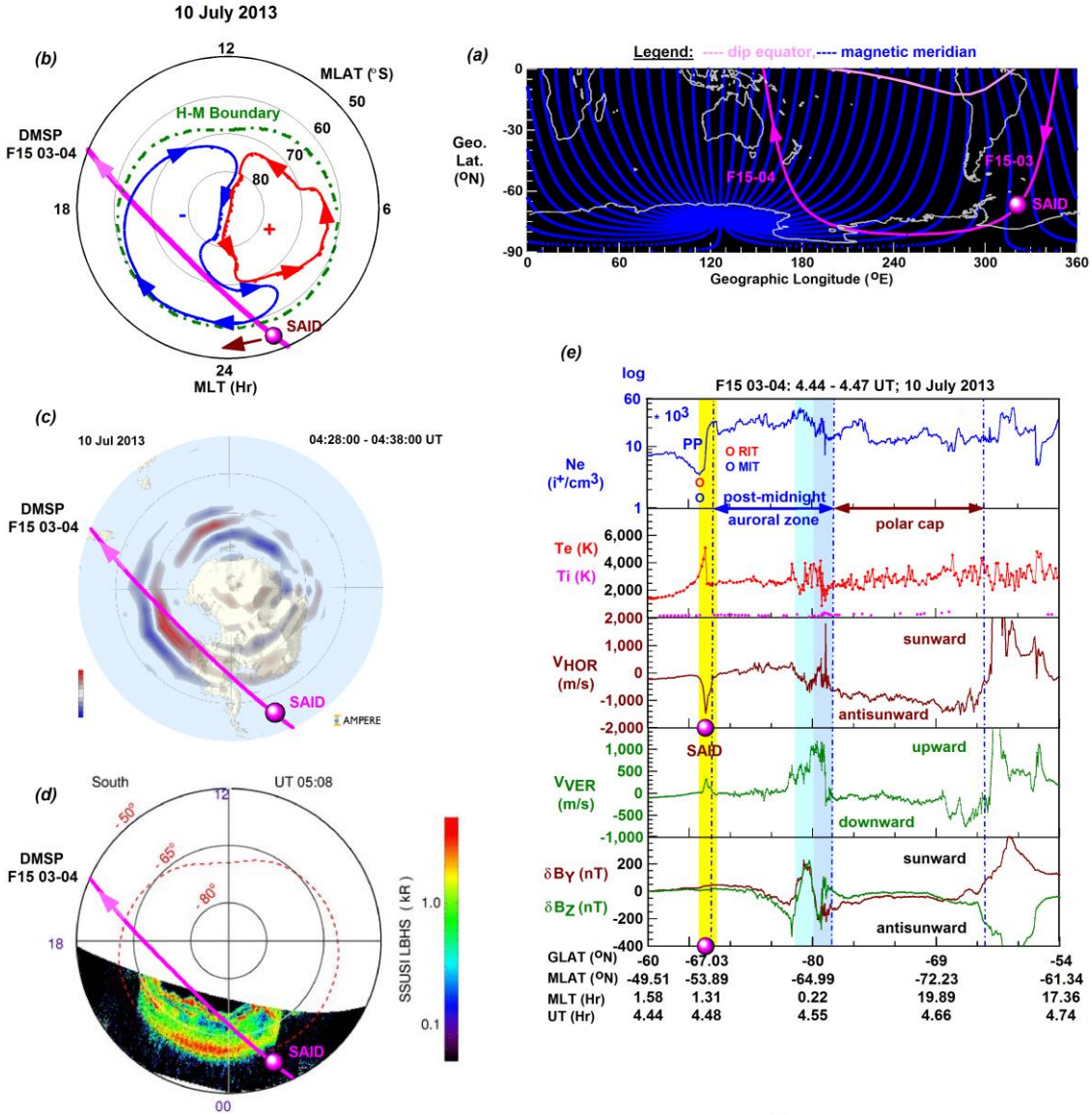

Figure 8 shows the 10 July 2013 antisunward streaming westward SAID event in the topside ionosphere when the westward SAID flow (driven by the poleward SAID E field) was streaming antisunward in concert with the dawnward intruding dusk cell related antisunward convection.

Figure 9 illustrates the 17 May 2013 antisunward (westward) SAID event. In panel (a), the southern-hemisphere map shows the satellite ground tracks of DMSP F15 and GOES (in colors), and also the antisunward (westward) SAID FC location (dot in green). In panel (b), the DMSP F15 line-plot sets depict the SAID FC (shaded interval in yellow) and its plasma environment including the dawn-cell-related strong sunward flows (shaded intervals in light orange) in the postmidnight auroral zone. In panel (c), the MLT versus MLAT polar plot shows the DMSP F15 and VAP satellite passes (in colors), the SAID FC and SAID E field locations (dots in colors), and the prevailing two-cell polar plasma convection characterized by a strong dusk cell extending into the dawnside. In panel (d), the orbit plots show the VAP and GOES orbit sections of interest and SAID-related locations (dots in colors). In panel (e), the VAP line-plot sets illustrate the steep plasmapause (PP), the outward SAID E field (shaded interval in yellow) and its plasma environment. In panel (f), the GOES line-plot sets depict the signatures of dispersionless particle injections just before the SAID detections (dots in colors, shaded interval in yellow). In the AU plot, the substorm onset is marked along with the SAID (dots in colors) and hot zone (shaded interval) detections. In panel (g), the VAP line-plot sets depict the hot zone tailward of the newly-formed plasmapause: in the regime of plasmasheet's earthward edge, the associated RC protons (in red) and energetic electrons (in light blue), the underlying temperature anisotropy and increased wave activity (in green and cyan), and the signatures of short-circuiting across the newly-formed plasmapause.

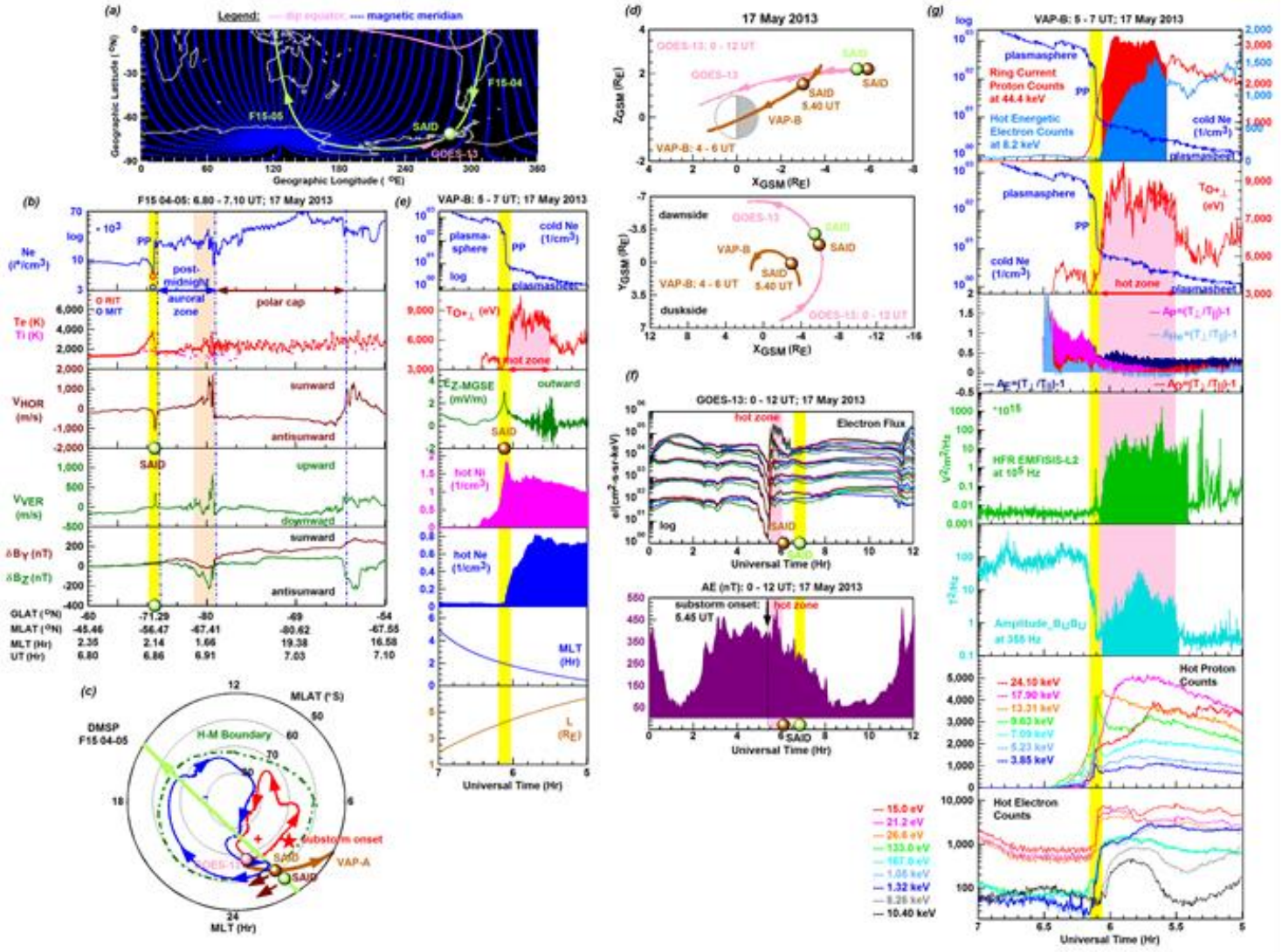

Figure 9 shows the 17 May 2013 antisunward streaming westward SAID event when the westward SAID flow (driven by the poleward SAID E field) was streaming antisunward in concert with the dawnward intruding dusk cell related antisunward convection and when the hot zone developed on the tailward side of the plasmapause: in the regime of plasmasheet's earthward edge.

Figure 10 illustrates the 24 June 2013 antisunward (westward) SAID event. Figure 10 is constructed the same way as Figure 9. Here, in Figure 10, we highlight some new features. These include, as shown in panel (b), the dawn-cell-related strong sunward flows (shaded interval in light orange) and also, shown in panel (g), the hot zone appearing earthward the newly-formed plasmapause (PP) in the regime of trapped energetic electrons (in light blue) within the plasmasphere and the localized heat source appearing across the newly-formed PP.

For the time period investigated we concluded that (i) different heating mechanisms became activated and generated localized heating leading to the development of the hot zone (earthward or tailward of the newly-formed plasmapause) and of (ii) the localized heat source (across the newly-formed plasmapause). Heating was generated by wave-particle interactions due to (a) the energetic particle population enhanced during short-circuiting, (b) the enhancement of low-frequency waves (including EMIC waves) and within the turbulent plasmaspheric boundary layer (TPBL) leading to SAR arc development on 1 June 2013) and/or (c) the amplification of auroral kilometric radiation (AKR) waves triggered by the instability of energetic electrons (of MPFs or BBFs) injected from the reconnection region.

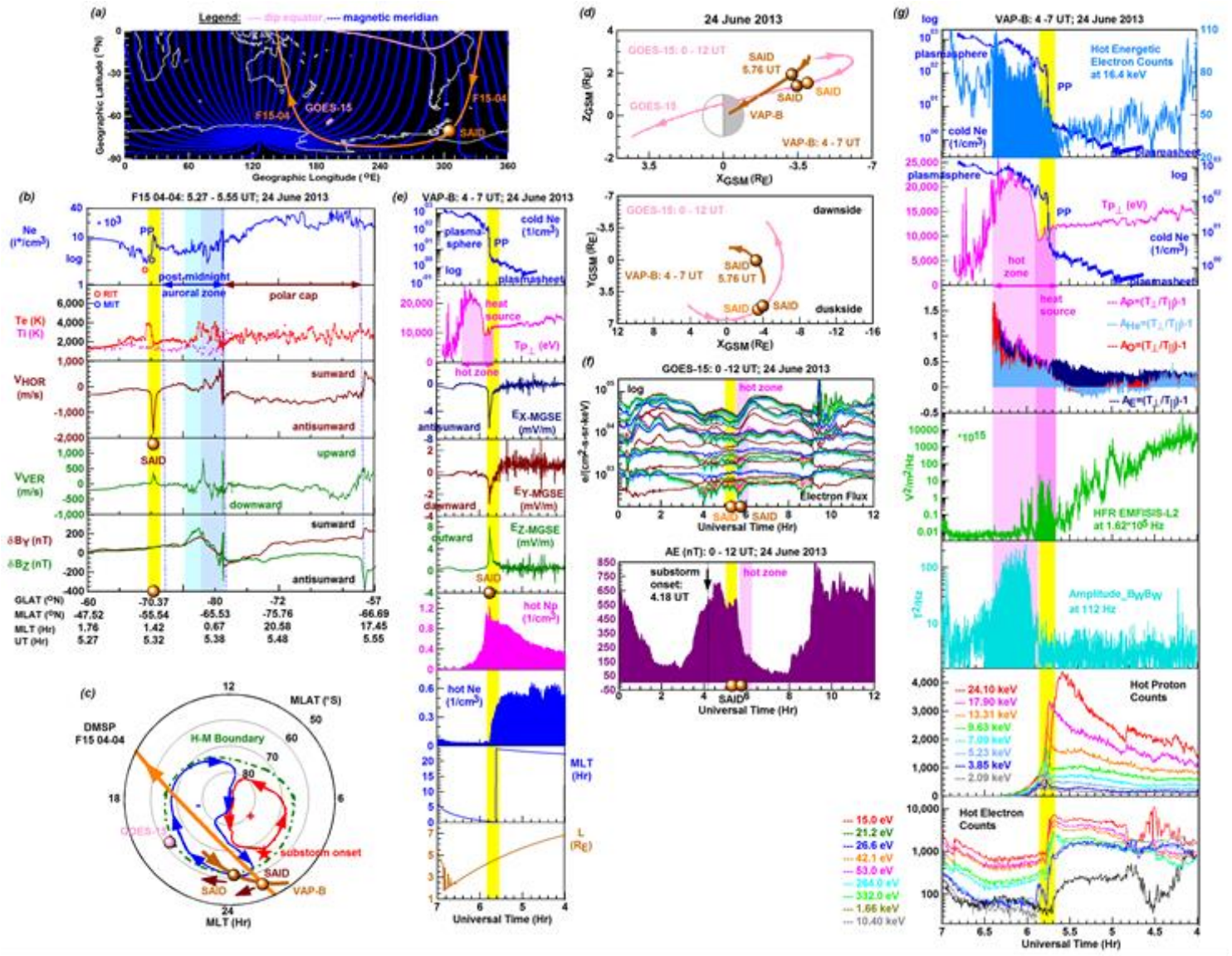

Figure 10 shows the 24 June 2013 antisunward streaming westward SAID event when the westward SAID flow (driven by the poleward SAID E field) was streaming antisunward in concert with the dawnward intruding dusk cell related antisunward convection and when the hot zone developed on the earthward side of the plasmapause: in the regime of trapped energetic electrons.

2.2.3.6 Abnormal Sub-Auroral Ion Drifts (ASAID) developed in the postmidnight (1-4) magnetic local time sector in 2013

In this study, we investigated the rare phenomenon of antisunward (eastward) ASAID FC occurring in the postmidnight (1-4) MLT sector of the topside ionosphere based on the 21 observations made by the DMSP F15 spacecraft during the calendar year of 2013. These observations provided the opportunity to investigate the antisunward (eastward) ASAID FC's various aspects, which have not been investigated before such the distribution of large-scale FACs observed by AMPERE, the underlying plasma density trough and auroral features (as shown in Figure 11), and M-I conjugacy along with the underlying generation mechanism of fast-time development by short-circuiting (Mishin & Puhl-Quinn, 2007; Mishin. 2013) applied to ASAID and the MPFs-associated auroral features (as shown in Figure 12).

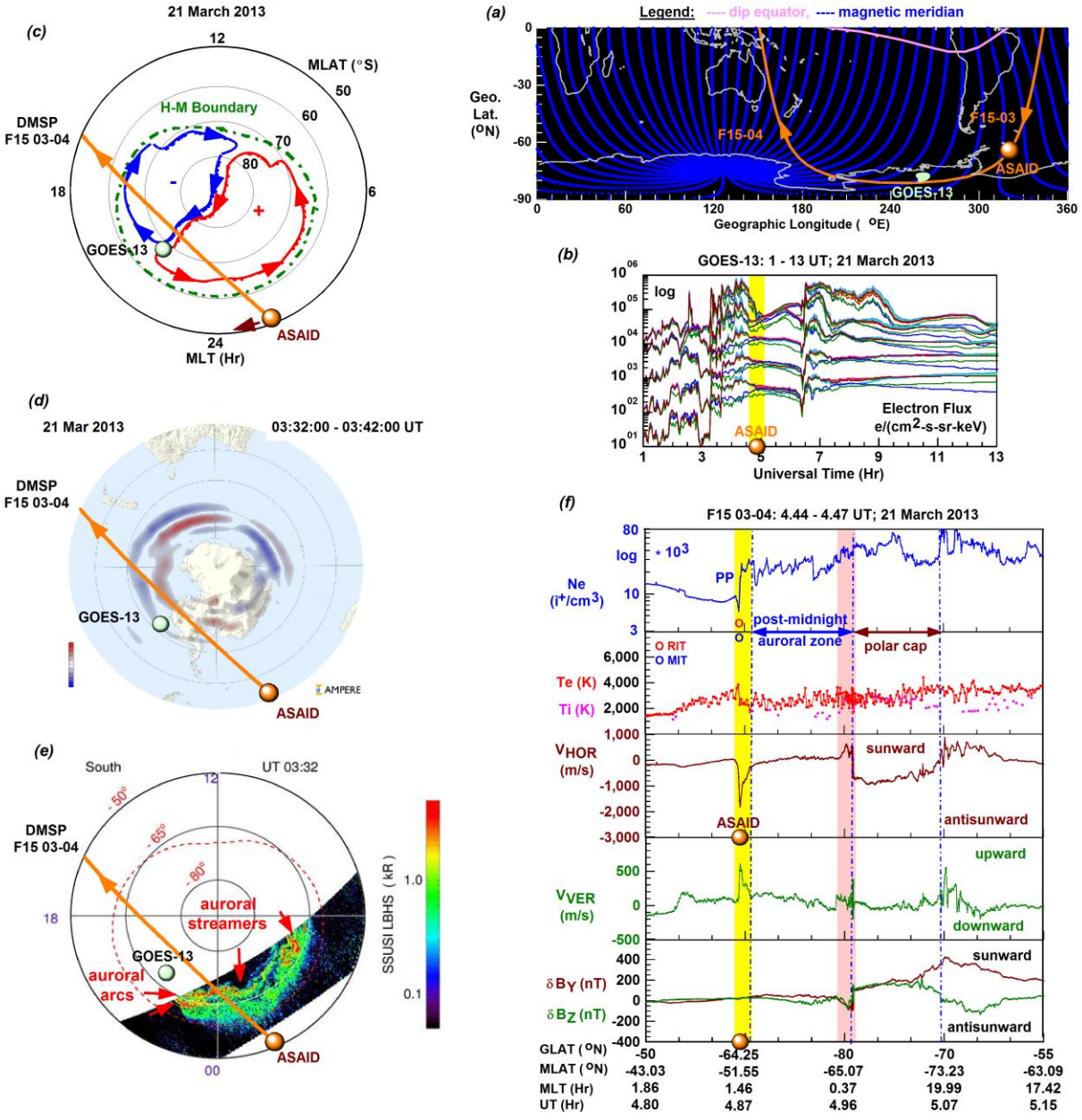

Figure 11 shows the 21 March 2013 antisunward streaming eastward ASAID event in the topside ionosphere when the eastward SAID flow (driven by the equatorward SAID E field) was streaming antisunward against the dawn cell related sunward convection.

Figure 11 is constructed for the antisunward streaming (eastward) ASAID FC detected on 21 March 2013 after midnight and illustrates the underlying polar convection, large-scale FAC distribution, and postmidnight auroral and plasma environment. In panel (a), the

southern-hemisphere map depicts the DMSP (in orange) descending F15-03 pass tracking the ASAID FC (dot in orange) near the South American continent and the ascending F15-04 pass near Australia, and the footprints of GOES-13 (in light green) during the time period of interest (1-13 UT). In panel (b), the GOES-13 line plots depict the signatures of substorm injections, characteristic to fast MPFs (Sergeev et al, 2014), just before the ASAID FC detection and thus imply the ASAID FC's fast-time development by short-circuiting. In panel (c), the MLT versus MLAT polar map illustrates the underlying tilted two-cell polar convection pattern. As shown, a smaller dusk cell (in blue) and a larger dawn cell (in red) developed with a convection axis tilted in the 9-21 MLT direction. This tilt shifted the dayside magnetopause reconnection site dawnward to ~9 MLT and the nightside magnetotail reconnection site duskward to ~21 MLT, where GOES-13 was located (dot in light green) and observed the magnetotail-reconnection-related dispersionless particle injections (shown in panel (b)) just before the ASAID detection. Here, in the postmidnight sector, the eastward ASAID flow was streaming antisunward, against the dawn cell related sunward convection. In panel (d), the AMPERE polar map shows that no R2 FACs had been flowing to subauroral latitudes and thus provide observational evidence that the ASAID FC developed independently of the large-scale R1-R2 FACs. In panel (e), the DMSP SUSSI image (taken near the time of the ASAID FC detection) depicts various auroral signatures. These include the signatures of (i) the dawn convection cell seen in the auroral precipitation since large-scale FACs are associated with both the polar convection cells and the auroral precipitation regimes (e.g. Wing et al., 2010), (ii) the auroral arcs developed near the poleward oval boundary, and (iii) the auroral streamers near the poleward auroral arc. Signatures (i) and (iii) provide observational evidence that the auroral convection flows were sunward directed in the postmidnight sector and that the antisunward (eastward) ASAID FC was quite newly-formed and developed soon after particle injections (as shown in panel (b)), since auroral streamers are the ionospheric footprints of BBFs/MPFs (Sergeev, et al., 1999). We mapped the GOES-13 location, the ground track of F15 03-04 pass, and the ASAID FC location illustrating the ASAID FC equatorward of the postmidnight auroral zone's precipitation regime. In panel (f), the DMSP F15 line-plot set depict the antisunward (eastward) ASAID FC (V_{HOR}=-1,810 m/s; dot in orange, shaded interval in yellow) with its underlying upward drift (V_{VER}=601 m/s), the enhanced sunward auroral flows (V_{HOR}=607 m/s; shaded interval in light red) associated with the above-described poleward auroral arc, and the polar cap region tracked in the premidnight (~0-20 MLT) sector. Showing no gradient change within the ASAID FC, the δB_Y and δB_Z line plots imply no large-scale FACs flowing into the subauroral region (as also shown by the above-described AMPERE image), since short-circuiting is not associated with large-scale R1-R2 FACs (Mishin, 2013).

Figure 12 shows the correlated closely in MLT and MLAT but loosely correlated in UT postmidnight observations made on 2 June 2013. In panel (a), the southern-hemisphere map shows the ground track of the DMSP (in light green) descending F15-04 pass over the South Atlantic where the antisunward (eastward) ASAID FC (marked as symbol dot in light green) was detected and the ascending F15-04 pass near Australia. In panel (b), the DMSP F15 line plots depict double plasmapause (PP) crossings characterized by the equatorward PP1 where Te peaked at ~4,500 K and by the poleward PP2 where the antisunward (eastward) ASAID FC (shaded interval in yellow) developed without any underlying large-scale FACs. In panel (c), the MLT versus MLAT polar map depicts the underlying two-cell convection pattern characterized by a significantly larger dawn cell than dusk cell and by a convection axis tilted in the 10-19 MLT direction. Here, we plotted the ground track of the DMSP F15 03-04 pass (in light green) and the VAP-B footprints (in dark orange) for the orbit section of interest, and also the closely located antisunward (eastward) ASAID FC (at 1.51 MLT; dot in light green) and inward (earthward) ASAID E field (at 1.07 MLT; dot in dark orange). These illustrate a close correlation in MLT and MLAT. But these ASAID features were observed at different universal times (at 4.32 UT by DMSP F15 and at 1.20 UT by VAP-B) making the correlation loose in term of UT detection. Panel (d) shows the AE index covering a 12-hour time period. Here we marked the ASAID detections (dots in colors; shaded intervals in yellow) and the onsets of the two consecutive

substorms occurring. While VAP-B observed the inward (earthward) ASAID E field between the two substorm onsets, DMSP F15 observed the antisunward (eastward) ASAID FC after the second substorm onset. Thus, these detections were made during different substorms. But these loosely correlated in UT but closely correlated in MLT and MLAT detections still provide observational evidence of the M-I conjugate ASAID phenomenon. Possibly, VAP-B observed a newly-formed inward (earthward) ASAID E field still showing the signatures of short-circuiting and DMSP F15 observed an earlier formed but still existing antisunward (eastward) ASAID FC.

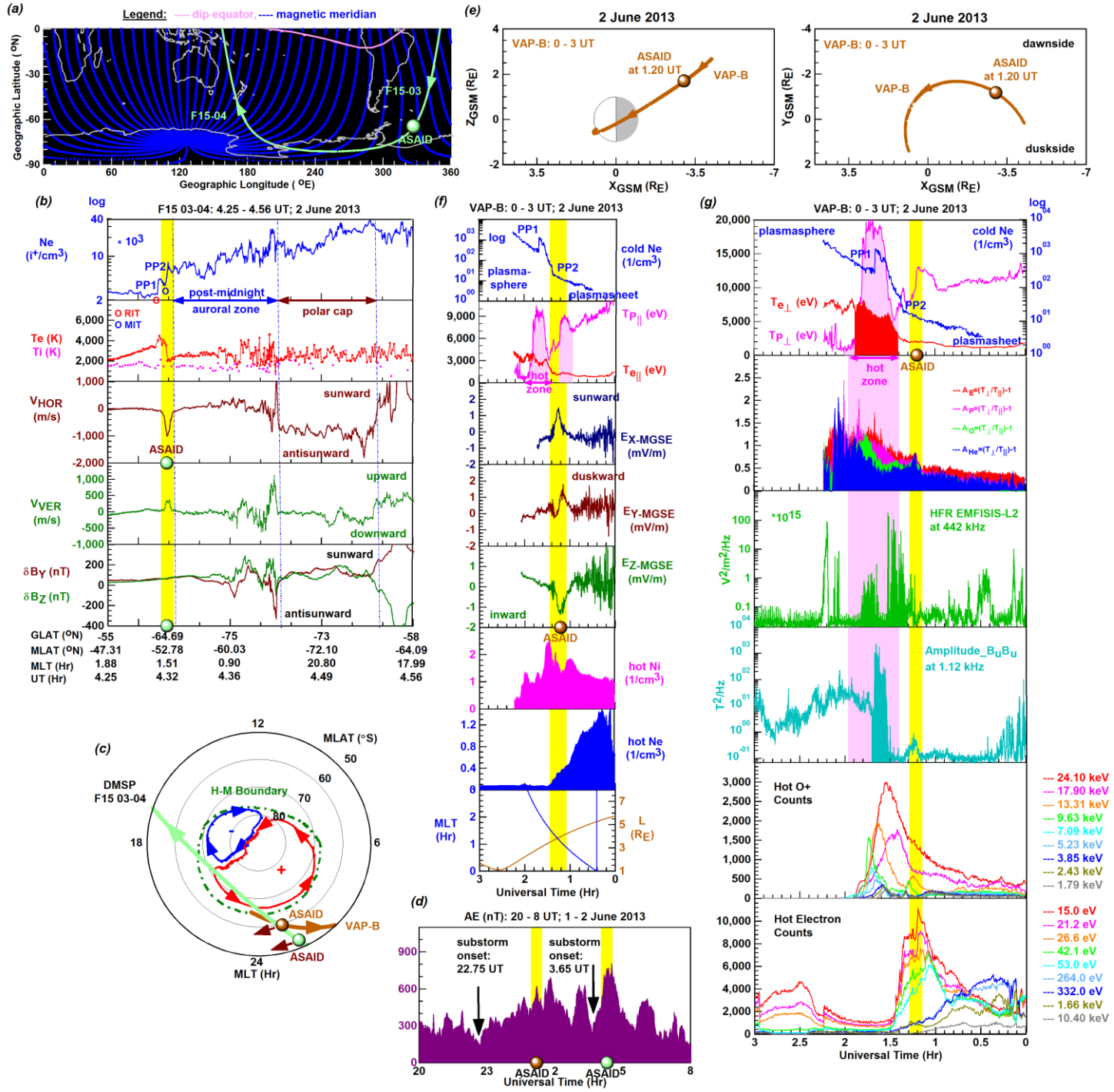

Figure 12 shows the 2 June 2013 antisunward streaming eastward ASAID event when the eastward ASAID flow (driven by the equatorward ASAID E field) was streaming antisunward against the dawn cell related sunward convection and when the hot zone developed across the plasmapause.

In panel (e), the orbit plots depict the VAP-B (in dark orange) orbit sections of interest and show that VAP-B observed the inward (earthward) ASAID E field (dot in dark orange) above the magnetic equatorial plane on the nightside and on the dawnside. In panel (f), the VAP-B line plots

show close similarities to their respective DMSP F15 observations. The inner-magnetosphere cold Ne plot shows that VAP-B also made double plasmapause crossings where the parallel (with the magnetic field lines) proton and electron temperature ($Tp_{\|}$ and $Te_{\|}$) increased at the inner (or earthward) PP1 (like Te peaked at the equatorward PP1 in the topside ionosphere). Meanwhile, $Tp_{\|}$ peaked again but $Te_{\|}$ remained minimum at the outer (or tailward) PP2 where the inward (earthward) ASAID E field developed (like Te minimized at the poleward PP2 where the antisunward (eastward) ASAID FC developed in the topside ionosphere). The localized increase of hot proton temperature at each plasmapause (PP1; PP2) was caused by the earthward intrusion of magnetized hot ring current protons (leading to the development of the hot zone across PP1) during the process of short-circuiting. Thus, this scenario demonstrates the hot-ring-current—cold-plasmasphere interface generating the development of the inward (earthward) ASAID E field via the finite Larmor radius effects activated (Voiculescu & Roth, 2008) because of the magnetized hot ring current protons. Panel (g) illustrates the hot zone (shaded in light magenta) in more detail. As shown, the hot zone developed in a region characterized by both maximum temperature anisotropy ($A \approx 1$ in this event) and Ti enhancement ($Ti > Te$). Thus, the possible mechanisms of heating ions occurred in the turbulent plasma (near PP1) and include induced scattering by EMIC waves along with the active waves specified as AKR waves.

From the results obtained, we draw the following conclusions (i-iv) for the time period investigated. (i) The antisunward (eastward) ASAID FC's close associations with the SAR arc via the elevated Te fueled by the hot zone. (ii) The strong differences between the fast-time development of inner-magnetosphere outward SAID E field and inward (earthward) ASAID E field created by their respective demagnetized and magnetized hot ions and associated infinite and finite Larmor radius effects. In agreement with previous studies (Voiculescu & Roth, 2008; Voiculescu; 2012), (iii) inner-magnetosphere ASAID development occurred in the hot-ring-current—cold-plasmasphere interface (Voiculescu, 2012) where the finite Larmor radius effect becomes dominant (Voiculescu & Roth, 2008), which (as shown in this study) (iv) unfolded during short-circuiting.

2.2.3.7 Intense westward Sub-Auroral Polarization Streams (SAPS) developed in the premidnight-postmidnight (23-2) magnetic local time sector during 2015 and 2016

In this study, we investigated the development of intense westward SAPS flows near magnetic midnight (23-2 MLT) based on the 24 SAPS observations made by the DMSP F15 spacecraft in the topside ionosphere during the calendar years of 2015 and 2016 and based on the 4 correlated M-I conjugate observations. These SAPS events depict (i) the intense near-midnight westward SAPS flows streaming mostly antisunward (as shown in Figure 13) but sometimes sunward (as shown in Figure 14) in the Harang region's vicinity, the M-I conjugate phenomena of (ii) SAPS and (iii) Harang reversal and (iv) associated features including the inner-magnetosphere hot zone and AKR waves as shown in Figure 13. Generated for the 4 correlated SAPS events and for the DMSP altitude of 840 km, (iv) the SAMI3 simulations reproduced the intense westward SAPS channel along with its underlying plasma environment: the deep plasma density trough and the elevated Te in the topside ionosphere (as shown in Figure 14).

Figure 13 shows the 18 February 2016 antisunward (westward) SAPS event depicting the westward SAPS flow streaming antisunward after magnetic midnight. The locations of DMSP F16 03-03 passes (in light red) and antisunward (westward) SAPS FC (dot in light red) are shown by a series of maps. In panel (a), the southern-hemisphere map depicts the SAPS FC south of Africa. In panel (b), the DMSP F15 time series depict the plasma environment of the SAPS FC (shaded interval in yellow) and the elevated Te reaching ~7,000 K and thus suggesting SAR arc development. In panel (c), the AMPERE image shows the large-scale upward (in red) and downward (in blue) FAC pattern with dawnward R2 currents near the SAPS FC as required by the development of westward SAPS (Mishin, 2013; Mishin et al., 2017). In panel (d) the DMSP SSUSI image shows the auroral precipitation in the dusk cell and the SAPS FC located equatorward of the auroral precipitation regime. In panel (e), the MLT versus MLAT polar maps illustrate the

polar two-cell convection pattern with the westward SAPS FC streaming antisunward equatorward of the dawnward intruding dusk cell (which is the ionospheric signature of the Harang reversal) and therefore in concert with the dawnward intruding dusk cell related convection.

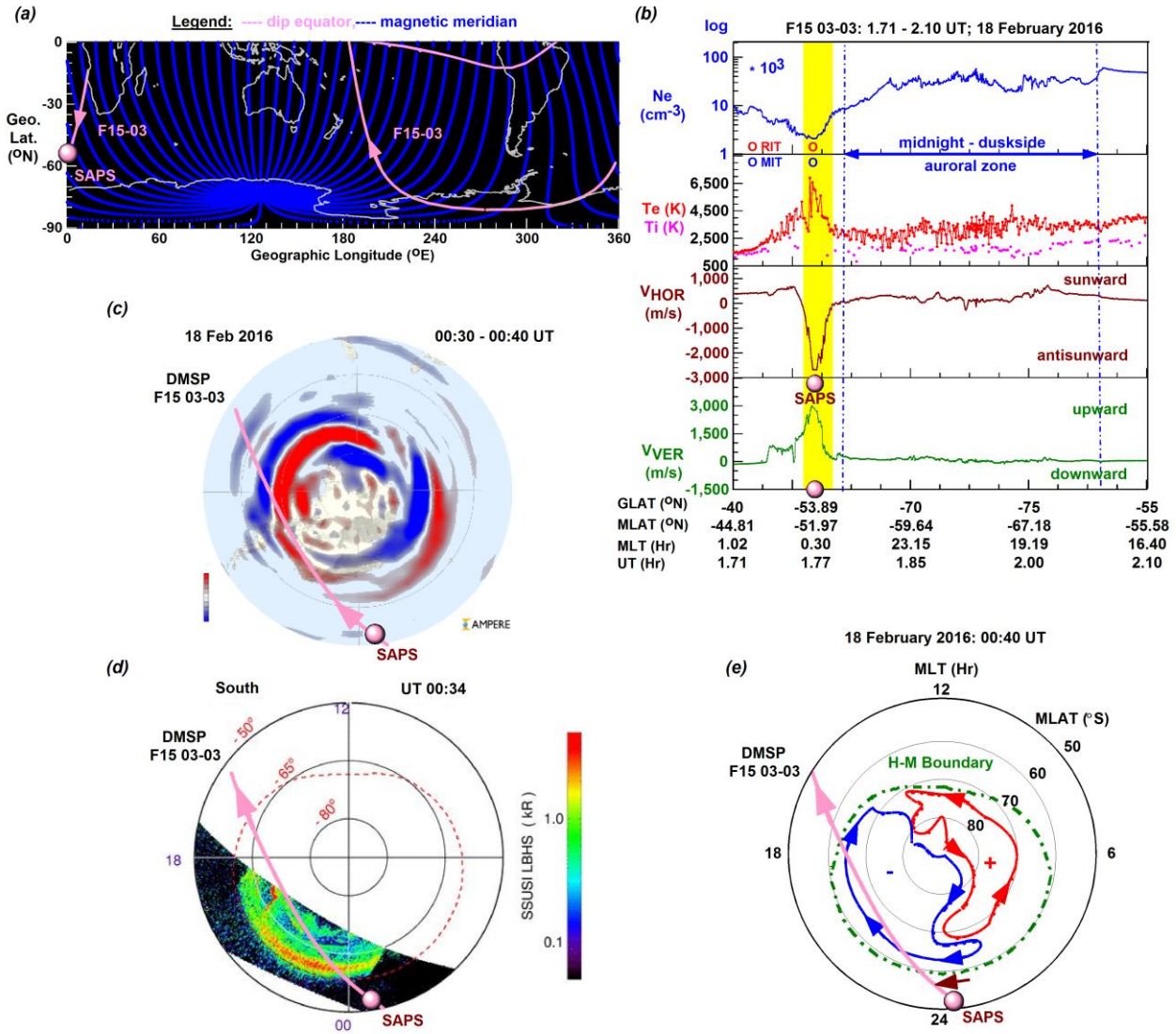

Figure 13 shows the 18 February 2016 antisunward streaming westward SAPS event in the topside ionosphere when the westward SAPS flow (driven by the poleward SAPS E field) was streaming antisunward in concert with the dawnward intruding dusk cell related antisunward convection.

Figure 14 illustrates the 20 September 2015 sunward (westward) SAPS event. In panel (a), the southern-hemisphere map shows the satellite ground tracks of DMSP F15 (in light blue) and THEMIS-A (TH-A; in orange), and also the locations of the ionospheric sunward (westward) SAPS FC (dot in orange) and the inner-magnetosphere outward SAPS E field (dot in light blue) and inward convection E field (E_C; symbol star in light blue). In panel (b), the DMSP F15 line-plot sets depict the sunward (westward) SAPS FC (shaded interval in yellow) and its plasma environment including the elevated Te reaching ~6,500 K implying SAR arc development. In panel (c), we show two sets of MLT versus MLAT polar plots. In the left panel, the polar plot depicts the prevailing two-cell polar plasma convection during the earlier observed sunward (westward) SAPS FC that developed at the tip of the dusk cell where the westward SAPS flow was streaming sunward in concert with the dusk cell related convection. In the right panel, the polar plot depicts the prevailing two-cell polar plasma convection during the later observed inner-magnetosphere Harang reversal when the Harang reversal mapped down from the inner magnetosphere to the dawnward intruding dusk cell in the ionosphere. In panel (d), the orbit plots

depict the TH-A orbit sections of interest with the TH-A-observed outward SAPS E field (E_{SAPS}) and inward convection E field (E_C) located above the magnetic equatorial plane and on the dawnside. In panel (e), the TH-A line-plot sets illustrate the steep plasmapause (PP), the Harang reversal characterized by the outward SAPS E field (shaded interval in yellow) associated with downward R2 FACs and inward convection E field (shaded interval in gray) associated with upward R2 FACs (Gkioulidou et al., 2009, 2011), and the plasma environment depicting the hot zone within the region of the Harang reversal and the signatures of short-circuiting across the steep (newly-formed) plasmapause. As the Ve line plots show, the electron drift increased locally (shaded interval in cyan) near the steep Ne gradient (depicted by the hot Ne plot), where the hot electron population of the earthward traveling MPFs became stopped (during the process of short-circuiting leading to fast-time SAPS development). At this stopping point, near the PP, the locally increased electron drift drove electron diamagnetic currents that excited various waves such as electrostatic ion-cyclotron (EIC) waves, fast magnetosonic (MS) waves and EMIC waves (Mishin et al., 2010; 2017; Mishin & Streltsov, 2021) generating heat in the hot zone by wave-particle interactions.

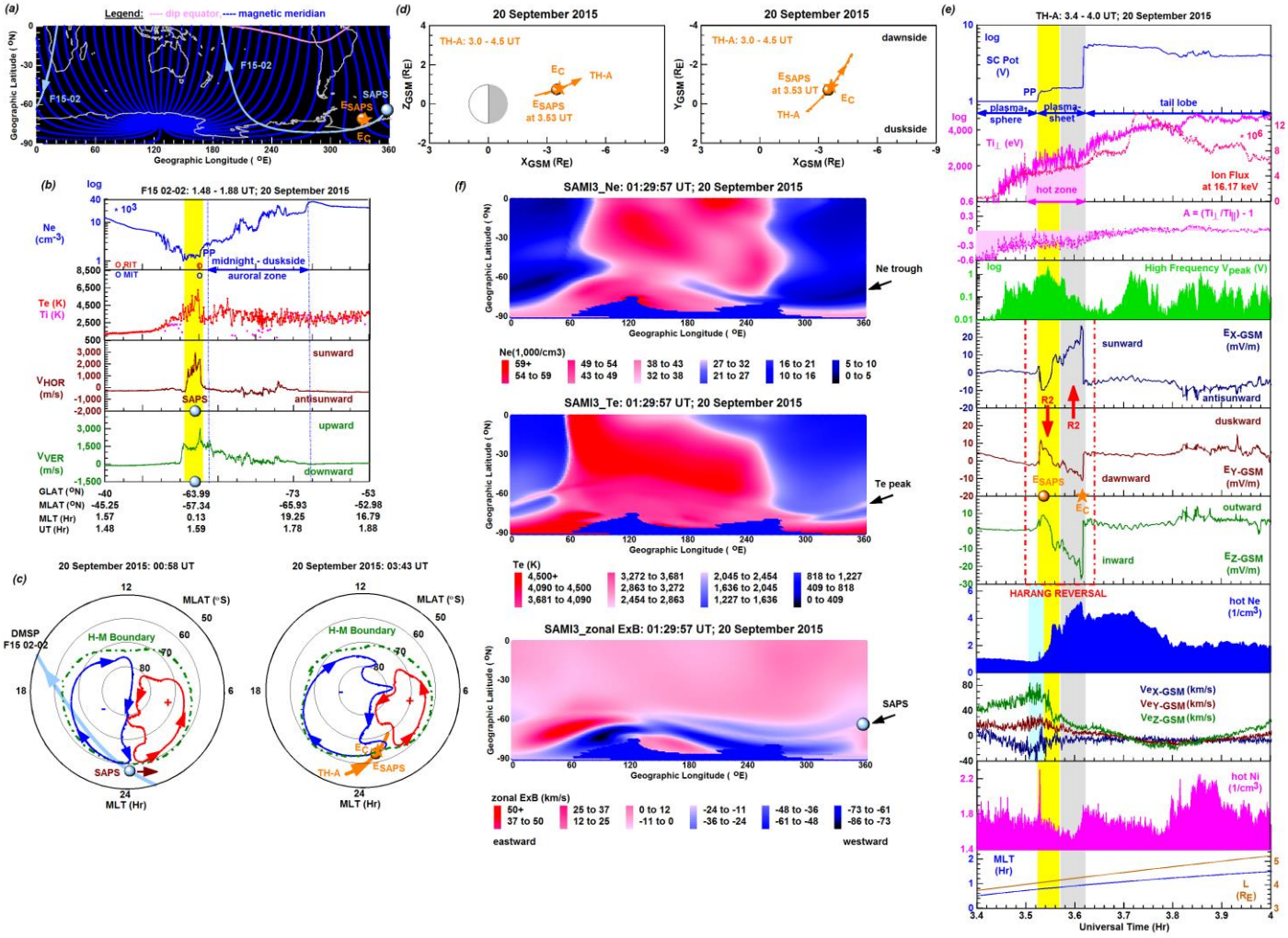

Figure 14 shows the 20 September 2015 sunward streaming westward SAPS event when the westward SAPS flow (driven by the poleward SAPS E field) was streaming sunward in concert with the dusk cell related sunward convection and when the hot zone developed on the tailward side of the plasmapause: within the Harang reversal region.

In panel (f), we show the SAMI3 simulated variables of Ne, Te, and zonal E×B drift generated for the DMSP altitude of 850 km and mapped over the southern hemisphere. We marked the DMSP F15-observed SAPS location (as arrow in black). Over the zonal E×B drift map, we also plotted (as dot in light blue) the DMSP F15-observed SAPS location showing a close correlation with the SAMI3 simulated SAPS location. These SAMI3 simulations reveal that the deep Ne trough (0 to $5*10^3$ cm^{-3}; black) developed both in the African (0-60 °E) and in the South Atlantic

(300-360 ^{o}E) longitude sectors. These are the longitude sectors where the MLT was near midnight during the UT hours of interest and where the DMSP F15 spacecraft observed (along its descending passes) the SAPS event. Within the deep Ne trough, Te became elevated (~3,000 K; shades of red) and the westward (-) zonal E×B drift (0 to -11 km/s; light red) -reproducing the intense westward SAPS flow channel- appeared

From the results obtained we concluded for the westward SAPS events investigated that the intense near-midnight westward SAPS flow (a) developed because of the strong inner-magnetosphere outward SAPS E field development in the Harang reversal region (where the upward-downward R2 FACs overlap) and (b) was amplified by the combined effects of deep plasma density trough and enhanced convections/return flows near the Harang (i.e. convection) reversal region.

References:

Anderson, P. C., Carpenter, D. L., Tsuruda, K., Mukai, T., & Rich, F. J. (2001). Multisatellite observations of rapid subauroral ion drifts (SAID). *Journal of Geophysical Research, 106(A12)*, 29,585-29,599. https://doi.org/10.1029/2001JA000128

Birn, J., Raeder, J., Wang, Y. L., Wolf, R. A., & Hesse, M. (2004). On the propagation of bubbles in the geomagnetic tail. *Annales Geophysicae, 22(5)*, 1,773-1,786. https://doi.org/10.5194/angeo-22-1773-2004

Décréau, P. M. E., Béghin, C., & Parrot, M. (1982). Global characteristics of the cold plasma in the equatorial plasmapause region as deduced from the Geos 1 Mutual Impedance Probe. *Journal of Geophysical Research, 87(A2)*, 695-712. https://doi.org/10.1029/JA087iA02p00695

Fairfield, D. H., Mukai, T., Brittnacher, M., Reeves, G. D., Kokubun, S., Parks, G. K., Nagai, T., et al. (1999). Earthward flow bursts in the inner magnetotail and their relation to auroral brightenings, AKR intensifications, geosynchronous particle injections and magnetic activity. *Journal of Geophysical Research: Space Physics, 104(A1)*, 355-370. https://doi.org/10.1029/98ja02661

Fok, M.-C., Moore, T. E., & Greenspan, M. E. (1996). Ring current development during storm main phase. *Journal of Geophysical Research, 101(A7)*,15,311-15,322. https://doi.org/10.1029/96ja01274

Foster, J. C., & Burke, W. J. (2002). SAPS: A new categorization for sub-auroral electric fields. *Eos, Transactions American Geophysical Union, 83(36)*, 393–394. https://doi.org/10.1029/2002EO000289

Frank, L. A. (1971). Relationship of the plasma sheet, ring current, trapping boundary, and plasmapause near the magnetic equator and local midnight. *Journal of Geophysical Research, 76(10)*, 2,265-2,275. https://doi.org/10.1029/JA076i010p02265

Gkioulidou, M., Wang, C.-P., Lyons, L. R., & Wolf, R. A. (2009). Formation of the Harang reversal and its dependence on plasma sheet conditions: Rice convection model simulations. *Journal of Geophysical Research, 114(A7)*, A07204. https://doi.org/10.1029/2008JA013955

Gkioulidou, M., Wang, C.-P., & Lyons, L. R. (2011). Effect of self-consistent magnetic field on plasma sheet penetration to the inner magnetosphere: Rice convection model simulations combined with modified Dungey force-balanced magnetic field solver. *Journal of Geophysical Research, 116(A12),* A12213. https://doi.org/10.1029/2011JA016810

Gringauz, K. I., & Bezrukikh, V. V. (1976). Asymmetry of the Earth's plasmasphere in the direction noon-midnight from Prognoz and Prognoz-2 data. *Journal of Atmospheric and Terrestrial Physics, 38(11)*, 1,071-1,076. https://doi.org/10.1016/0021-9169(76)90036-2

He, F., Zhang, X.-X., Wang, W., & Chen, B. (2016). Double-peak subauroral ion drifts (DSAIDs). *Geophysical Research Letters, 43(11)*, 5554-5562. https://doi.org/10.1002/2016GL069133

Heilig, B., Stolle, C., Kervalishvili, G., Rauberg, J., Miyoshi, Y., Tsuchiya, F., et al. (2022). Relation of the plasmapause to the midlatitude ionospheric trough, the sub-auroral temperature enhancement and the distribution of small-scale field aligned currents as observed in the magnetosphere by THEMIS, RBSP, and Arase, and in the topside ionosphere by Swarm.

Journal of Geophysical Research: Space Physics, 127(3), e2021JA029646. https://doi.org/10.1029/2021JA029646

Horvath, I., & Lovell, B. C. (2019a). Investigating the development of abnormal subauroral ion drifts (ASAID) during the magnetically quiet times of October 2003. *Journal of Geophysical Research: Space Physics, 124(1),* 715-733. https://doi.org/10.1029/2018JA026230

Horvath, I., & Lovell, B. C. (2019b). Abnormal subauroral ion drifts (ASAID) and Pi2s during cross-tail current disruptions observed by Polar on the magnetically quiet days of October 2003. *Journal of Geophysical Research: Space Physics, 124(7),* 6097-6116. https://doi.org/10.1029/2019JA026725

Jacobs, J., & Watanabe, T. (1964). Micropulsation whistlers. *Journal of Atmospheric and Terrestrial Physics, 26(8),* 825-826. https://doi:10.1016/0021-9169(64)90180-1

Keiling, A., Angelopoulos, V., Runov, A., Weygand, J., Apatenkov, S. V., Mende, S., et al. (2009). Substorm current wedge driven by plasma flow vortices: THEMIS observations. *Journal of Geophysical Research, 114(A1),* A00C22. https://doi.org/10.1029/2009ja014114

Kozyra, J. U., Jordanova, V. K., Home, R. B., & Thorne, R. M. (1997). Modeling of the contribution of electromagnetic ion cyclotron (EMIC) waves to stormtime ring current erosion. *Magnetic Storms, Geophysical Monograph Series*. (Vol. 98, pp. 187-202). Washington, DC: American Geophysical Union. https://doi.org/10.1029/GM098p0187

Leonovich, A. S., & Mazur, V. A. (2005). Letter to the Editor: Why do ultra-low-frequency MHD oscillations with a discrete spectrum exist in the magnetosphere? *Annales Geophysicae, 23(3),* 1,075-1,079. https://doi.org/10.5194/angeo-23-1075-2005

Lyons, L. R., Nagai, T., Blanchard, G. T., Samson, J. C., Yamamoto, T., Mukai, T., et al. (1999). Association between GEOTAIL plasma flows and auroral poleward boundary intensifications observed by CANOPUS photometers. *Journal of Geophysical Research, 104(A3),* 4,485-4,500. https://doi.org/10.1029/1998JA900140

Maynard, N. C., Burke, W. J., Basinska, E. M., Erickson, G. M., Hughes, W. J., Singer, H. J., Yahnin, A. G., Hardy, D. A., & Mozer, F. S. (1996). Dynamics of the inner magnetosphere near times of substorm onsets. *Journal of Geophysical Research, 101(A4),* 7705-7736. https://doi:10.1029/95JA03856

Mishin, E. V. (2013). Interaction of substorm injections with the subauroral geospace: 1. Multispacecraft observations of SAID. *Journal of Geophysical Research: Space Physics, 118(9),* 5,782-5,796. https://doi.org/10.1002/jgra.50548

Mishin, E. V., & Puhl-Quinn, P. A. (2007). SAID: Plasmaspheric short circuit of substorm injections. *Geophysical Research Letters, 34(24),* L24101. https://doi.org/10.1029/2007GL031925

Mishin, E., & Blaunstein, N. (2008). Irregularities within subauroral polarization stream-related troughs and GPS radio interference at midlatitudes. In P. M. Kintner Jr., A. J. Coster, T. Fuller-Rowell, A. J. Mannucci, M. Mendillo, & R. Heelis (Eds.), *MidLatitude ionospheric dynamics and disturbances* (Vol. 181, pp. 291-295). Geophysical Monograph Series. https://doi.org/10.1029/181GM26

Mishin, E. V., Puhl-Quinn, P. A., & Santolik, O. (2010). SAID: A turbulent plasmaspheric boundary layer. *Geophysical Research Letters, 37(7),* L07106. https://doi.org/10.1029/2010GL042929

Mishin, E., Nishimura, Y., & Foster, J. (2017). SAPS/SAID revisited: A causal relation to the substorm current wedge. *Journal of Geophysical Research: Space Physics, 122(8),* 8,516-8,535. https://doi.org/10.1002/2017JA024263

Mishin, E. & Sotnikov, V. (2017). The turbulent plasmasphere boundary layer and the outer radiation belt boundary. *Plasma Physics and Controlled Fusion, 59(12),*124003. https://doi.org. /10.1088/1361-6587/aa8481

Mishin, E., & Streltsov, A. (2019). STEVE and the picket fence: Evidence of feedback-unstable magnetosphere-ionosphere interaction. *Geophysical Research Letters, 46(24),* 14,247-14,255. https://doi.org/10.1029/2019gl085446

Mishin, E., & Streltsov, A. (2020). Prebreakup arc intensification due to short circuiting of mesoscale plasma flows over the plasmapause. *Journal of Geophysical Research: Space Physics, 125(5),* e2019JA027666. https://doi.org/10.1029/2019JA027666

Mishin, E., & Streltsov, A. (2021). Mesoscale and Small-Scale Structure of the Subauroral Geospace. In Huang, C., &. Lu, G. (Eds.), *Space Physics and Aeronomy Collection Volume 3:* Ionosphere Dynamics and Applications, Geophysical Monograph Series (Vol 260, pp.135-154) Washington DC: American Geophysical Union. https://doi.org/10.1002/9781119815617.ch8

Nishimura, Y., Mrak, S., Semeter, J. L., Coster, A. J., Jayachandran, P. T., Groves, K. M., et al. (2021). Evolution of mid-latitude density irregularities and scintillation in North America during the 7–8 September 2017 storm. *Journal of Geophysical Research: Space Physics, 126(6),* e2021JA029192. https://doi.org/10.1029/2021JA029192

Nishimura, Y., Dyer, A., Kangas, L., Donovan, E., & Angelopoulos, V. (2023). Unsolved problems in strong thermal emission velocity Enhancement (STEVE) and the picket fence. *Frontiers in Astronomy and Space Sciences, 10,* 1087974. https://doi.org/10.3389/fspas.2023.1087974

Puhl-Quinn, P. A., Matsui, H., Mishin, E., Mouikis, C., Kistler, L., Khotyaintsev, Y., et al. (2007). Cluster and DMSP observations of SAID electric fields. *Journal of Geophysical Research, 112(A5),* A05219. https://doi.org/10.1029/2006JA012065

Ruohoniemi, J. M., & Greenwald, R. A. (2005). Dependencies of high-latitude plasma convection: Consideration of interplanetary magnetic field, seasonal, and universal time factors in statistical patterns. *Journal of Geophysical Research, 110(A9)*. A09204. https://doi.org/10.1029/2004ja010815

Sinevich, A., Chernyshov, A., Chugunin, D., Clausen, L. B. N., Miloch, W. J., & Mogilevsky, M. M. (2023). *Stratified subauroral ion drift (SSAID). Journal of Geophysical Research: Space Physics, 128(3),* e2022JA031109. https://doi.org/10.1029/2022JA031109

Spiro, R. W., Heelis, R. A., & Hanson, W. B. (1979). Rapid subauroral drifts observed by Atmosphere Explorer C. *Geophysical Research Letter, 6(8),* 657-660. https://doi.org/10.1029/GL006i008p00657

Sergeev, V. A., Liou, K., Meng, C. I., Newell, P. T., Brittnacher, M., Parks, G., & Reeves, G. D. (1999). Development of auroral streamers in association with localized impulsive injections to the inner magnetotail. *Geophysical Research Letters, 26(3),* 417-420. https://doi.org/10.1029/1998GL900311

Sergeev, V. A., Nikolaev, A. V., Tsyganenko, N. A., Angelopoulos, V., Runov, A. V., Singer, H. J., & Yang, J. (2014). Testing a two-loop pattern of the substorm current wedge (SCW2L). *Journal of Geophysical Research, 119(2)*. 947-963. https://doi:10.1002/2013JA019629

Su, Z., Liu, N., Zheng, H., Wang, Y., & Wang, S. (2018). Multipoint observations of nightside plasmaspheric hiss generated by substorm-injected electrons. *Geophysical Research Letters, 45(20),* 10,921-10,932. https://doi.org/10.1029/2018GL079927

Summers, D., Thorne, R. M., & Xiao, F. (1998). Relativistic theory of wave-particle resonant diffusion with application to electron acceleration in the magnetosphere. *Journal of Geophysical Research, 103(A9),* 20487-20500. https://doi.org/10.1029/98ja01740

Troitskaya, V., & Gul'Elmi, A. (1967). Geomagnetic micropulsations and diagnostics of the Magnetosphere. *Space Science Reviews, 7(5-6),* 689-768. https://doi.org/10.1007/BF00542894

Usanova, M. E., Mann, I. R., Kale, Z. C., Rae, I. J., Sydora, R. D., Sandanger, M., et al. (2010). Conjugate ground and multisatellite observations of compression-related EMIC Pc1 waves and associated proton precipitation. *Journal of Geophysical Research, 115(A7),* A07208. https://doi.org/10.1029/2009JA014935

Vlasov, M. N., & Tashkinova, L. G. (1981). Interpretation of the ion temperature measurements in the outer plasmasphere. *Advances in Space Research, 1(1),* 185-187. https://doi.org/10.1016/0273-1177(81)90105-8

Voiculescu, M. (2012). Ionospheric perturbations induced by interplanetary and solar forcing. International Conference SOLAR AND HELIOSPERIC INFLUENCES ON THE GEOSPACE, Bucharest, ROMANIA, 1 – 5 October 2012

URL:www.geodin.ro/CONFERENCE2012/.../Iono_perturb_solar_mag_forcing_tosend.pdf
Voiculescu, M. & Roth, M. (2008). Eastward sub-auroral ion drifts or ASAID. *Annales Geophysicae, 26(7),* 1955-1963. https://doi.org/10.5194/angeo-26-1955-2008
Wing, S., Ohtani, S., Newell, P. T., Higuchi, T., Ueno, G., & Weygand, J. M. (2010). Dayside field-aligned current source regions. *Journal of Geophysical Research, 115(A12),* A12215, https://doi.org/10.1029/2010JA015837.
Yumoto, K., & Saito, T. (1980). Hydromagnetic waves driven by velocity shear instability in the magnetospheric boundary layer. *Planetary and Space Science, 28(8),* 789-798. https://doi.org/10.1016/0032-0633(80)90076-8

2.3 How were the results disseminated to communities of interest?

All the major results of this project are documented in journal articles published by the Journal of Geophysical Research Space Physics. The PI had regular communications and active email interactions with Dr. E. V. Mishin (AFRL/RVBXI) throughout the project.

3. Impacts

Demonstrating the significance of the results obtained and the contribution of these new results to the community knowledge base, one of the published articles [Horvath, I., & Lovell, B. C. (2023). Antisunward streaming westward sub-auroral ion drifts (SAID) developed in the postmidnight (1-4) magnetic local time sector during 2013. *Journal of Geophysical Research: Space Physics, 128(9),* e2023JA031677. https://doi.org/10.1029/2023JA031677] was featured as an Editor's Highlight in the recently published Eos Science News: Probing Rare Hot Plasma Flows in the Upper Atmosphere Postmidnight flows appear to be triggered by the same mechanism that drives more frequently observed evening flows.
(ttps://eos.org/research-spotlights/probing-rare-hot-plasma-flows-in-the-upper-atmosphere)

4. Changes

4.1 Changes in approach

There was changes in approach.

4.2 Problems or delays

There were delays in the reviewing process with the manuscripts submitted.

4.3 Expenditure Impacts

N/A

4.4 Significant changes in the use or care of human subjects, vertebrate animals and/or biohazards

N/A

4.5 Changes to the primary place of performance from that originally proposed

N/A

5. Technical Updates

The PI had regular email contact with the acting AOARD Program Manager, Dr. Kim (earlier) and Dr. Andersen (later on). Throughout the project, the PI sent copies of the manuscripts to be submitted, updates on manuscript submissions and acceptance, and information on newly published articles.

6. Future follow-on project

Our follow-on project will be focused on subauroral flow channel development during the midnight and postmidnight and dawn magnetic local time (MLT) hours. These MLT sectors,

including the dawn sector, are less intensively investigated and therefore less understood. It is still not clear how the various subauroral flows (such as SAPS) develop in the near midnight MLT sector and how the strong polar convection contributes to their development. Since the strong postmidnight polar convection is associated with the Harang reversal, we will study how the strong polar convection (along with the Harang reversal) promote subauroral flow channel development. Correlated magnetosphere-ionosphere (M-I) conjugate observations will be analyzed for the underlying magnetosphere driver mechanisms and also for the hot zone playing a key role in subauroral flow channel development.